

The American Journal of Pathology

Development of a novel model of central retinal vascular occlusion and the therapeutic potential of the adrenomedullin-RAMP2 system

Kazutaka Hirabayashi^{1,2}, Masaaki Tanaka^{1,2}, Akira Imai^{1,2}, Yuichi Toriyama^{1,2},
Yasuhiro Iesato^{1,2}, Takayuki Sakurai¹, Akiko Kamiyoshi¹, Yuka Ichikawa-Shindo¹,
Hisaka Kawate¹, Megumu Tanaka¹, Kun Dai¹, Nanqi Cui¹, Yangxuan Wei¹,
Keisei Nakamura¹, Shiho Iida¹, Shuhei Matsui^{1,3}, Akihiro Yamauchi⁴,
Toshinori Murata², Takayuki Shindo¹

¹Department of Cardiovascular Research, Shinshu University Graduate School of Medicine, Japan

²Department of Ophthalmology, Shinshu University School of Medicine, Japan

³Department of Anesthesiology, Shinshu University School of Medicine, Japan

⁴Japan Bio Products Co., Ltd., Tokyo, Japan

Short running head: *Adm-Ramp2* system suppresses CRVO

Number of text pages 47
Number of tables 1
Number of figures 14
Number of supplementary figures 4

Disclosures: Akihiro Yamauchi is an employee of Japan Bio Products Co., Ltd

Sources of funding

This study was supported by Grant-in-Aid for Scientific Research (KAKENHI), Core Research for Evolutionary Science and Technology (CREST) of Japan Science and Technology Agency (JST) and the Japan Agency for Medical Research and Development (AMED), National Cardiovascular Center grant for cardiovascular diseases, Takeda Medical Research Foundation grant; SENSHIN Medical Research Foundation grant, Naito Foundation grant, NOVARTIS Foundation (Japan) for the Promotion of Science grant and Bristol-Myers Squibb research grand for T.S.

Address for correspondence

Takayuki Shindo, MD, PhD

Department of Cardiovascular Disease,

Shinshu University Graduate School of Medicine

Asahi 3-1-1, Matsumoto, Nagano, 390-8621, Japan

Tel: +81-263-37-2578

Fax: +81-263-37-3437

Email: tshindo@shinshu-u.ac.jp

Abstract

Central retinal vein occlusion (CRVO) is an intractable disease that causes visual acuity loss with retinal ischemia, hemorrhage and edema. In this study, we developed an experimental CRVO model in mice and evaluated the therapeutic potential of the pleiotropic peptide adrenomedullin (ADM) and its receptor activity-modifying protein, RAMP2. The CRVO model, which had phenotypes resembling those seen in the clinic, was produced by combining intraperitoneal injection of Rose Bengal, a photo-activator dye enhancing thrombus formation, with laser photocoagulation. Retinal vascular area, analyzed using fluorescein angiography and fluorescein isothiocyanate-perfused retinal flat-mounts, was decreased after induction of CRVO but gradually recovered from day 1 to 7. Measurements of retinal thickness using optical coherence tomography and histology revealed prominent edema early after CRVO followed by gradual atrophy. Reperfusion after CRVO was diminished in *Adm* and *Ramp2* knockout (KO) mice, but was increased by exogenous ADM administration. CRVO also increased expression of a coagulation factor, oxidative stress markers and a leukocyte adhesion molecule in both wild-type and *Adm* KO mice, and the effect was more pronounced in *Adm* KO mice. Using retinal capillary endothelial cells, we found that ADM directly suppresses retinal endothelial injury. Based on these findings, we propose that the retinoprotective effects of the *Adm-Ramp2* system make it a novel therapeutic target for treatment of CRVO.

Abbreviations

RVO; retinal vein occlusion

CRVO; central retinal vein occlusion

BRVO; branch retinal vein occlusion

DR; diabetic retinopathy

OCT; optical coherence tomography

VEGF; vascular endothelial growth factor

ADM; adrenomedullin

CLR; calcitonin receptor-like receptor

RAMP; receptor activity-modifying protein

KO; knockout

WT; wild-type

FA; fluorescein angiography

FITC; fluorescein isothiocyanate

Keywords

central retinal vein occlusion; adrenomedullin; RAMP2; genetically engineered mice

Introduction

Retinal vein occlusion (RVO) is the second most common retinal vascular disease, the first being diabetic retinopathy (DR)¹. Obstruction of the retinal vein is commonly caused by thrombus formation, which can occur as a complication associated with hypertension, diabetic mellitus and dyslipidemia, among others. RVO can be subdivided into central retinal vein occlusion (CRVO) and branch retinal vein occlusion (BRVO) based on the site of the occlusion. In both of cases, retinal capillary dropout, ischemia, macular edema and vascular complications initiated by the occlusion can lead to severe visual loss. But despite its relatively high prevalence, substantial controversy still surrounds the pathophysiology of RVO².

The fundamental molecular pathogenesis of RVO is still under discussion, though vascular endothelial growth factor (VEGF) is thought to be a key player. This is because VEGF promotes hyperpermeability and inflammation of the retinal vasculature, as well as neovascularization. In recent years, intravitreal administration of anti-VEGF agents has been used to treat RVO³; however, this approach has several associated drawbacks. One is recurrence of macular edema; another is tachyphylaxis, which can occur after long-term anti-VEGF administration^{4,5}. And finally, anti-VEGF agents may not fully reverse the functional and structural damage caused by RVO. For those reasons, identification of other therapeutic targets involved in controlling vascular integrity would be desirable.

Originally isolated from human pheochromocytoma, adrenomedullin (ADM) is a vasodilating polypeptide whose expression is upregulated under ischemic conditions⁶⁻⁸. We previously showed that homozygous *Adm* knockout (*Adm*^{-/-}) mice die *in utero* due to

vascular structural abnormalities⁹, which is indicative of ADM's indispensability for proper vascular development. Moreover, ADM also exerts vascular effects in adults^{9,10}, and it is now known to be widely distributed in numerous tissues and organs and to exert a variety of physiological effects in addition to vasodilatation. For example, ADM also exerts antioxidant, anti-inflammatory, antifibrotic and anti-apoptotic effects^{11,12,13}. The main body of the ADM receptor is calcitonin receptor-like receptor (CLR), a 7-transmembrane domain G protein-coupled receptor. CLR associates with 1 of 3 subtypes of receptor activity-modifying protein (RAMP), which determines the affinity of CLR for its ligands^{14, 15}. In that regard, we showed that homozygous *Ramp2* knockout (*Ramp2*^{-/-}) mice die *in utero* and exhibit a phenotype similar to that of *Adm*^{-/-} mice, which suggests the *Adm-Ramp2* system is specifically involved in vascular development¹⁶.

Adm expression has been also detected in the eye. In earlier reports, ADM was shown to act as a vasodilator in the retinal arteries and to increase choroidal blood flow and ophthalmic arterial flow velocity^{17,18}. In addition, ADM levels are elevated in the vitreous fluid of DR patients¹⁹⁻²¹, and plasma and vitreous ADM levels are reportedly related to the severity and stability of DR^{21,22}. Collectively, these findings suggest ADM is involved in the pathophysiology of ocular diseases. Consistent with that idea, we demonstrated that the *Adm-Ramp2* system is crucially involved in retinal angiogenesis using an oxygen-induced retinopathy model with heterozygous *Adm* and *Ramp2* knockout (KO) mice^{23, 24}. More recently, we reported that exogenous administration of ADM suppresses vascular hyperpermeability and inflammation in a DR model²⁵. These observations prompted us to investigate the relationship between ADM and CRVO.

An animal model could help us to understand the precise pathophysiology of CRVO, which could serve as the basis for development of new treatments. However, there is currently no standard animal model in which the phenotypic characteristics exactly mimic human CRVO. This mainly reflects the complexity of the pathological changes occurring along the time course of CRVO. Nevertheless, several animal models of vascular occlusion using laser photocoagulation, photodynamic coagulation, intravitreal injection of dermal fibroblasts, and diathermic cauterization have been proposed²⁶. Among them, the photodynamic coagulation method²⁷ shows early features of the clinical disease, including retinal capillary dropout, hemorrhage and edema. In the present study, we developed an easy and reproducible model of CRVO in mice, which is particularly useful when analyzing genetically modified mice. Using this model, we analyzed the sequential events occurring in CRVO, including capillary dropout, ischemia, macular edema and inflammation, and then assessed the potential of ADM to serve as a therapeutic agent for the treatment of CRVO.

Materials and Methods

Animals

Adm and *Ramp2* knockout mice (KO) were previously generated in our group^{9, 16}. But because homozygous *Adm* or *Ramp2* KO is embryonically lethal, we used heterozygous *Adm* and *Ramp2* KO mice. In these mice, expression of the affected genes is reduced to about half that in wild-type (WT) mice. Used in this study were 9- to 12-week-old male *Adm* KO, *Ramp2* KO and WT mice, as well as WT mice systemically administered ADM using an osmotic pump. The background of all the mice was C57BL/6J. Before the operative procedures, the mice were anesthetized through intraperitoneal injection of a combination anesthetic that included 0.3 mg/kg of medetomidine (Nippon Zenyaku Kogyo Co.Ltd., Koriyama Japan), 4.0 mg/kg of midazolam (Astellas Pharma Inc. Tokyo Japan) and 5.0 mg/kg of butorphanol (Meiji Seika Pharma Co.Ltd., Tokyo Japan).

All animal handling procedures were in accordance with a protocol approved by the Ethics Committee of Shinshu University School of Medicine. All experiments were performed in accordance with the Association for the Research in Vision and Ophthalmology's Statement for the Use of Animals in Ophthalmic and Vision Research and our institutional guidelines.

Administration of ADM to mice

Human ADM (Peptide Institute, Inc., Osaka, Japan) dissolved in phosphate-buffered saline (PBS) was infused into subcutaneous tissues using osmotic pumps (Alzet,

DURECT Co., Cupertino, CA). The delivery rate was 29 $\mu\text{g}/\text{kg}/\text{day}$, and the mice received ADM for 7 days. Mice treated with PBS served as controls.

Intravitreal administration of ADM to mice

For subsequent study of CD68- and CD206-immunostained retinal flat-mount preparations, human ADM dissolved in PBS (10^{-5} M ; 1.0 μl) was intravitreally injected at the temporal corneoscleral junction using a Hamilton syringe fitted with a 32-gauge needle under a stereoscopic surgical microscope. As a control, eyes were intravitreally injected with 1.0 μl of PBS. After the procedure, the mice were administered moxifloxacin hydrochloride antibiotic drops (Vegamox Ophthalmic Solution, Alcon, Fudenberg, Switzerland).

Photodynamic coagulation method

CRVO was induced in the right eye of each mouse. After anesthesia, 40 mg/kg Rose Bengal (FUJIFILM Wako Pure Chemical Corporation, Osaka, Japan) was intraperitoneally injected. The pupil was then dilated with 1 drop of 0.5% tropicamide and 0.5% phenylephrine (Mydrine P, Santen, Osaka, Japan). Photodynamic coagulation was induced using a green laser slit-lamp delivery system (GYC-1000; NIDEK, Gamagori, Japan) with a cover slip serving as a contact lens. The wavelength was 532 nm, the power was 50 mW, the duration was 3 s, and the spot size was 50 μm and positioned at the optic disc. Photocoagulation was repeated several times until central

retinal vein occlusion was confirmed. After the CRVO procedure, 3.0 mg/kg atipamezole (ZEOAQ, Fukushima, Japan) was intraperitoneally injected

Fluorescence angiography (FA)

On days 1, 3 and 7 after induction of CRVO, mice were anesthetized, and the cornea was kept moist using saline. Mice were then manually held in front of a fundus camera (TRC-50AX, Topcon, Tokyo, Japan), and FA was performed after intraperitoneal injection of 12 μ L/g 2.5% fluorescein sodium (Alcon, Freiburg, Germany). Images were taken after 1-3 min of fluorescein perfusion and used for quantitative evaluations. Vascular density, vascular area and vascular branch points were quantified from the FA images using AngioTool image analysis software version 0.6a (National Cancer Institute, MD).

Fluorescein isothiocyanate (FITC)-dextran perfusion and retinal flat-mount

On day 7 after induction of CRVO, mice were anesthetized and perfused with 1 ml of PBS containing 50 mg/ml FITC-labeled dextran (MW 2×10^6) (Sigma-Aldrich, St. Louis, MO) via the left ventricle. The eyes were then enucleated and fixed for 1 h in 4% paraformaldehyde, after which the cornea and lens were removed, and the entire retina was carefully dissected from the eyecup. Four radial cuts were then made from the edge to the equator, and the eyecup (retina) was flat-mounted with the scleral side facing down and examined using a fluorescence microscope. Images of whole mount retinas were taken using a fluorescence microscope (BZ-9000, Keyence, Osaka, Japan). Vascular area

was quantified from the FITC images using AngioTool image analysis software.

Topical endoscopy fundus imaging

Topical endoscopy fundus imaging was performed as described previously²⁸ with some modifications. We used an endoscope coupled to a 5-cm-long otoscope with a 3-mm outer diameter (1218AA; Karl Storz, Tuttlingen, Germany). A reflex digital camera with an 18-megapixel CMOS image sensor (EOS REBEL T4i, Canon, Tokyo, Japan) was connected to the endoscope through an adapter. Pupils were dilated using topical 0.5% phenylephrine and 0.5% tropicamide (Mydrin-P; Santen, Osaka, Japan), which were respectively applied 60 min and 30 min prior to eye examination. Mice were anesthetized just before the examination, after which their whiskers were shaved, and one drop of 0.4% oxybuprocaine (Nitto Medic, Tokyo, Japan) was applied to each eye. The camera was placed on a platform, and the endoscope was slowly moved toward the mouse. Once the endoscope was in contact with the gel covering the cornea, the photographer adjusted its position by horizontally displacing the tip. Focus and illumination were adjusted during examination of the fundus through the camera.

Measurement of retinal edema using optical coherence tomography (OCT)

OCT imaging was performed to evaluate retinal edema after induction of CRVO. Envisu R-Class OCT (Leica Microsystems, Wetzlar, Germany) and Heidelberg SPECTRALIS OCT (Heidelberg Engineering GmbH, Heidelberg, Germany) were used. With Envisu R-Class OCT, retina thickness at 0.25 mm from the optic disc was measured

before and after CRVO (days 1-20). With Heidelberg SPECTRALIS OCT, the Heidelberg Eye Explorer (Heidelberg Engineering GmbH) segmentation algorithm was applied, which recognizes the internal limiting membrane (ILM) and the basal membrane. Segmentation was confirmed by visual observation, and manual adjustments were made when the ILM and basement membrane clearly deviated. For analysis of retinal thickness, a standard ETDRS grid with circle diameters of 1 mm, 3 mm, and 6 mm was centered on the optic nerve head. Retinal volume within a region 6 mm in diameter was automatically calculated. Retinal volume was measured before and after CRVO (days 1-7, 11, 14, 18 and 21). OCT angiography was also performed using a SPECTRALIS OCT angiography module (Heidelberg Engineering GmbH) before and after CRVO (days 7 and 21).

Isolectin B4 staining

Retinas were isolated and stained overnight at 4°C with Alexa Fluor 568-conjugated *Griffonia bandeiraea simplicifolia* isolectin B4 (Thermo Fisher Scientific, Waltham, MA) in PBS with 0.3% Triton X-100 (1:200 dilution). After washing three times in PBS, the retinas were whole-mounted with the photoreceptor side down on microscope slides and embedded in fluorescence mounting medium (Agilent Technologies, Santa Clara, CA). Images of whole-mount retinas were taken using a fluorescence microscope (BZ-9000, Keyence).

Immunohistochemistry

Mice were sacrificed and retinal flat-mounts were made as described above. After blocking with 1% bovine serum albumin, the flat-mounts were stained using rat anti-mouse F4/80 antibody (BIO-RAD, Hercules, CA), rat anti-mouse CD68 antibody (Abcam, Cambridge, UK) or rabbit anti-mouse CD206 antibody (Abcam), which were then reacted with appropriate secondary antibodies. CD68- or CD206-positive cells were then counted in multiple microscope fields.

Retinas were also fixed overnight in 4% paraformaldehyde, embedded in paraffin, and cut into 5- μ m-thick sections for HE-staining and immunohistological analysis of rabbit anti-mouse p67phox antibody (Merck Millipore, Darmstadt, Germany). Images of whole-mount retinas and sections were taken using a fluorescence microscope (BZ-9000, Keyence).

Real-time RT-PCR array analysis

We used a PCR array (RT² Profiler PCR Array, QIAGEN, Hilden, Germany) to assess expression of a focused panel of genes. After 1 μ g of total RNA of retina was converted to cDNA using a RT² First Strand Kit (QIAGEN), levels of specific transcripts were assessed using a Mouse Angiogenesis and Mouse Endothelial Cell Biology PCR Array (QIAGEN) according to the manufacturer's protocols. All PCR reactions were run using a StepOnePlus Real-Time PCR System (Thermo Fisher Scientific). RT² Profiler PCR Array data were analyzed using RT² Profiler Array Data Analysis version 3.5 software.

Quantitative real-time RT-PCR analysis

Total RNA was isolated from the retina using a PureLink RNA Mini Kit (Thermo Fisher Scientific). RNA quality was then verified using electrophoresis, and concentrations were measured using an Oubit 3.0 fluorometer (Thermo Fisher Scientific). Thereafter, the extracted RNA was treated with DNA-Free (Thermo Fisher Scientific) to remove contaminating DNA, and 2- μ g samples were subjected to reverse transcription using a PrimeScript™ RT reagent Kit (Takara Bio, Shiga, Japan). Quantitative real-time RT-PCR was carried out using a StepOne Plus Real-Time PCR System (Thermo Fisher Scientific) with SYBR green (Toyobo, Osaka, Japan) or Realtime PCR Master Mix (Toyobo) and TaqMan probe (MBL, Nagoya, Japan). Values were normalized to mouse GAPDH expression (Pre-Developed TaqMan assay reagents, Thermo Fisher Scientific) or rat GAPDH expression (using primers synthesized for rat GAPDH expression). The primers used are listed in Table 1.

Endothelial cells

TR-iBRB cells (FACT, Sendai, Japan), a conditionally immortalized rat retinal capillary endothelial cell line generated from rats harboring temperature-sensitive SV40 antigen, were used for this study. TR-iBRB cells were cultivated on 24-well plates in DMEM supplemented with 10% fetal bovine serum (FBS) and antibiotics. Once the cells reached confluence, they were stimulated for 24 h using TNF- α (20 ng/ml) with or without ADM (10^{-7} , 10^{-9} M). Cells were then harvested and used for real-time PCR analysis.

Statistical analysis

Statistical analysis was performed using GraphPad Prism 7.04. (GraphPad Software Inc., CA). Values are expressed as means \pm SEM. Student's t test and one-way ANOVA followed by Dunnett's test were used to determine the significance of differences. Values of $p < 0.05$ were considered significant.

Results

Evaluation of vascular perfusion in the CRVO model

We induced CRVO using a previously described photodynamic coagulation method with some modification²⁷. As a sensitizing agent, we used intraperitoneally administered Rose Bengal. We then confirmed that the subsequent laser radiation efficiently induced photodynamic coagulation.

In fundus images acquired on day 7, we noted retinal hemorrhage as well as retinal vein dilatation with tortuousness in the treated mice (Figure 1A). Retinal flat-mount images also showed prominent hemorrhage in the treated mice (Figure 1B). Retinal hemorrhage is the most characteristic finding of clinical CRVO, and is not observed in central retinal artery occlusion (CRAO). This confirms that a CRVO model was successfully generated.

Fluorescein angiography (FA) was performed on days 1, 3 and 7 after CRVO. After injecting fluorescein isothiocyanate (FITC) via the heart, retinal flat mounts were prepared. FA revealed the percent vascular area of the retina to be 26% in untreated mice. On day 1 after CRVO, lack of vascular perfusion due to blood vessel occlusion was prominent, and the percent vascular area was only 2.7%. Thereafter, vascular perfusion gradually recovered over time, but the percent vascular retinal area remained below control on day 7 (day 3: 8.4%, day 7: 17%) (Figure 2A, B). FITC-perfused retinal flat-mounts also showed decreased vascular area on day 7 (untreated group: 53%, CRVO group: 30%) (Figure 2C, D).

Evaluation of retinal edema in the CRVO model using OCT and histology

We next used OCT to evaluate post-CRVO retinal edema. With color mapping using clinical OCT equipment (Heidelberg SPECTRALIS OCT), the degree of retinal edema was depicted from yellow to red, while retinal atrophy was depicted in blue (Figure 3A). On OCT B-scans, cross sections of the retina between the internal limiting membrane (ILM) and basement membrane (BM) were visualized (Figure 3B). The retinal volume within a region 6 mm in diameter around the optic disc was automatically calculated by the algorithm built into the OCT equipment (Figure 3C).

The retinal volume was 7.0 mm^3 in the no treatment group. Retinal edema was most prominent on day 1, and retinal volume reached 1.4 times the baseline level. Because of the edema, the structure of the inner layer of the retina became ambiguous on the B-scan. Thereafter, the retinal volume gradually declined to the baseline level by day 7 (7.2 mm^3). After Day 11, however, the retinal volume continued to decline to levels significantly below baseline. This retinal atrophy continued until day 21 (4.2 mm^3). We also analyzed the retinal thickness using OCT equipment for smaller experimental animals (Envisu R-Class OCT) and obtained similar results (Supplementary Figure 1, 2).

Using OCT angiography, we observed in untreated mice, smaller capillaries between the main retinal blood vessels radiating from the optic disc (arteries and veins) (Figure 4A, left panel). These smaller capillaries were undetectable on day 7 after CRVO, however, though the main retinal blood vessels were still well visualized at this stage (Figure 4A, middle panel). In B scans of the OCT angiography in untreated mice, blood flow signals were detected at both superficial and deep layers, which respectively

represent blood flow in the main retinal blood vessels and smaller capillaries (Figure 4B. left panel). The blood flow in the smaller capillaries in the deep layer was undetectable on day 7 after CRVO (Figure 4B. middle panel). These observations indicate that small capillary dropout is irreversible, though the main retinal blood vessels show reperfusion on day 7 after CRVO. By day 21 after CRVO, however, the main retinal blood vessels appeared shrunken (Figure 4A, right panel).

Histological changes to the retinal layer structure was examined in HE-stained cross-sections prepared from retinas with and without CRVO (days 1, 7 and 21) (Figure 4C). Retinal edema was prominent, especially at the inner layer of the retina from day 1 to day 7. On day 7, decudation of the cells in inner nuclear layer (INL) and abnormal cavity formation within the choroid were noticeable. On day 21, the inner retinal layer was undetectable, and only outer layers of the retina (outer plexiform layer (OPL) and outer nuclear layer (ONL) were detectable. These histological observations of retinal edema and atrophy correspond well to the OCT analysis.

Evaluation of macrophages and microglia in retinal flat-mounts

We have been using isolectin B4 staining to visualize endothelial cells in the retinal vasculature²⁵. Comparing images of FITC perfusion and isolectin B4 staining in retinal flat-mounts after CRVO, we noticed that the distributions of FITC and isolectin B4 positivity differed somewhat (Figure 5A). In images of FITC-perfused retinas, non-perfused areas could not be clearly visualized (Figure 5A left panel). On the other hand, isolectin B4-stained areas were detected in both perfused and non-perfused areas. We

think that isolectin B4 positivity without FITC perfusion is indicative of non-perfused vessels. Moreover, we found that isolectin B4 staining was much stronger in non-perfused than perfused areas (Figure 5A middle panel). Under higher magnification of nonperfused areas, we also observed isolectin B4 positivity in small round structures that were clearly different from vascular branch structures (Figure 5B, left panel), and some had dendrites. The round structures also stained positive for the macrophage marker F4/80 (Figure 5B, middle panel). Thus, macrophage numbers were increased in the non-perfused areas after induction of CRVO. This suggests inflammation is more severe in the non-perfused ischemic areas of the retina.

CD206 is a marker of M2 macrophages, while CD68 is a marker of macrophages and activated microglia²⁹. CD206-positive cells were mainly located in the inner layer of retina and are thought to be resident microglia. Percentages of CD206-positive microglia declined slightly after CRVO (Figure 5D). By contrast, CD68-positive cells were rarely observed before CRVO, but after CRVO their numbers increased over time, and they were distributed in all layers of the retina (Figure 5C, D). CD-68-positive cells were therefore thought to be either pro-inflammatory macrophages derived from outside of the retina or activated microglia, both of which are thought to be involved in retinal inflammation after CRVO.

Evaluation of the gene expression with and without CRVO

To further evaluate the pathogenesis of the CRVO model, we performed a real-time PCR array analysis of angiogenesis- and endothelial cell-related molecules in mouse

retinas with and without CRVO. The clustergrams in Figure 6A and B show the results of the analysis. Each column depicts the results from one mouse, while red and green colors represent higher and lower gene expression, respectively. All the examined mice in each group showed similar gene expression profiles. After induction of CRVO, expression levels of chemokines, growth factors and coagulation factors were higher than in the untreated group (Figure 6C, shown in red dots). On the other hand, some angiogenic factors, including *Fgfl*, *Mmp9*, *Nrp2*, *Igfl* and *Hgf*, were downregulated in the vascular occlusion group (Figure 6C, shown in green dots).

Analysis of the time-course of the gene expression revealed that the coagulation-related molecule *Serpine1* (PAI-1) was most prominently upregulated on day 3 after CRVO (52-fold) (Figure 7A). A leukocyte adhesion molecule, *Vcam-1*, was prominently upregulated (11-fold) on day 7 after CRVO. In association with the inflammatory reaction, the NADPH subunits *Ncf1* (p47phox) and *Ncf2* (p67phox) were also upregulated on day 7 (*Ncf1*: 8.5-fold, *Ncf2*: 11-fold), as was the macrophage and activated microglia marker *Cd68* (60-fold). These observations suggest enhanced coagulation, inflammation and oxidative stress are all involved in the pathogenesis of CRVO. We also found that *Adm* expression was significantly upregulated on days 1 (72-fold) and 3 (118-fold) after CRVO, but it had declined by day 7 (4.5-fold) (Figure 7B). *Adm*'s receptor, *Calcrl* (CLR) was most upregulated on day 3 (5.6-fold), while *Ramps* were upregulated on days 3 and 7. The timing of the dynamic changes in gene expression suggests ADM and its receptor system are crucially involved in the pathogenesis of CRVO.

***Adm* and *Ramp2* knockout mice show more severe phenotypes in the CRVO model**

To evaluate the role played by ADM in the pathophysiology of CRVO, we compared heterozygotic *Adm* and *Ramp2* KO mice to WT mice. In *Adm* KO mice, serum ADM was reduced to 70% of the level in wild-type mice (Supplementary Figure 3). FA showed that after CRVO in WT mice, the percent vascular area of the retina was initially decreased but gradually recovered from day 1 to 7 (Figure 8A, B). In *Adm* and *Ramp2* KO mice, there tended to be less recovery than in WT mice (*Adm* KO: day1, 1.3%; day 3, 5.9%; day 7, 15% and *Ramp2* KO: day 1, 0.75%; day 3, 3.0%; day 7, 14%). In addition, FITC-perfused retinal flat-mounts (Figure 8C, D) showed significantly less vascular area in *Adm* KO (13.0%) and *Ramp2* KO (17.0%) mice than in WT mice (30%).

Comparison of the retinal gene expression profiles of WT and *Adm* KO with and without CRVO revealed that the angiogenic factors *Nos3* (eNOS), *Tek* (Tie-2) and *Angpt1* were significantly upregulated in *Adm* KO at baseline (Figure 9A, upper left panel). As ADM has angiogenic properties, upregulation of these molecules is thought to be a compensatory response to the reduction in ADM. Levels of these angiogenic molecules also tended to be higher in *Adm* KO after CRVO (data not shown).

Comparison of *Serpine1* (PAI-1), *Cd68*, *Vcam-1*, *Ncf1* (p47phox) and *Ncf2* (p67phox) expression between WT and *Adm* KO mice showed that, even before CRVO, levels of *Serpine1*, *Cd68*, *Vcam-1* and *Ncf2* expression were significantly higher in *Adm* KO than WT mice (Figure 9A). Expression of *Ncf1* also tended to be elevated in *Adm* KO mice. As mentioned above, expression these genes were upregulated after CRVO, but the effect was much more pronounced in *Adm* KO mice. In retinal flat-mounts, we also found

that numbers of CD68-positive macrophages and activated microglia were higher in *Adm* KO than WT mice, while numbers of CD206-positive resident microglia were lower (Figure 9B). These observations suggest reducing *Adm* expression exacerbates inflammation and suppresses vascular reperfusion after CRVO. Thus, endogenous ADM likely exerts protective effects against the retinal damage caused by CRVO.

ADM administration ameliorates the phenotypes in the CRVO model

We next evaluated the therapeutic effects of exogenous ADM administration in the CRVO model. ADM was systemically administered using subcutaneous osmotic pumps. In ADM-administered mice, serum ADM was 50% higher than in wild-type mice. (Supplementary Figure 3). Both FA- and FITC-perfused retinal flat-mounts showed that vascular reperfusion after CRVO was increased by ADM administration (Figure 10A-D), while FITC-perfused flat-mounts showed that ADM significantly increased vascular area in (control: 30%, ADM administration: 45%). (Figure 10D). In a real-time PCR array analysis, we found that ADM administration upregulated several angiogenic factors and downregulated inflammation-related cytokines and chemokines (Supplementary Figure 4). ADM administration markedly suppressed expression of *Serpine1* (PAI-1), *Cd68*, *Vcam-1*, *Ncf1* (p47phox) and *Ncf2* (p67phox) (Figure 11A). In retinal flat-mounts, numbers of CD68-positive macrophages and activated microglia were decreased and CD206-positive resident microglia were increased after ADM administration (Figure 11B). In addition, expression of *Kdr* (VEGFR-2) was greatly elevated after CRVO (day 3: 7.9-fold, day 7: 9.8-fold), and that effect too was markedly suppressed by ADM

administration.

We also analyzed the cross-sectional histology of the retinal layers (Figure 12). On day 7 after CRVO, disruption of the inner retinal layer was exacerbated in *Adm* KO mice, and suppressed by ADM administration. Moreover, *Adm* KO mice showed elevated expression of *Ncf2* (p67phox), which is indicative of a higher level of oxidative stress. These observations suggest ADM administration ameliorates the pathology of CRVO by enhancing vascular reperfusion and suppressing both inflammation and oxidative stress.

ADM directly suppresses retinal endothelial injury

Given the effects of ADM summarized above, we speculated that ADM suppresses vascular injury after CRVO. To test that idea, we assessed the effect of ADM administration on TR-iBRB cells, an immortalized retinal capillary endothelial cell line. To induce endothelial injury, the cells were stimulated for 24 h with 20 ng/ml TNF- α in the presence or absence of ADM (10^{-7} - 10^{-9} M). Subsequent quantitative real-time PCR analysis showed that expression of inflammatory and oxidative stress-related molecules (*Vcam-1*, *Ccl2* (MCP-1), *Cd68*, *Ncf1* (p47phox), and *Ncf2* (p67phox)) was highly upregulated by TNF- α administration, but co-administration of ADM downregulated that expression (Figure 13). ADM administration also downregulated expression of *Kdr* (VEGFR-2). These observations corresponded well to the results obtained with the CRVO model and suggest ADM exerts direct protective effects against retinal endothelial cell injury.

Discussion

RVO affects an estimated 16.4 million people worldwide and is one of the most common retinal vascular diseases in adults, second only to DR¹. In CRVO, venous dilatation with tortuosity, hemorrhage and edema occur in association with venous occlusion. There are two types of CRVO, ischemic and non-ischemic³⁰, with the ischemic type being refractory to treatment³¹. Capillary dropout is a key feature of ischemic RVO, and when it occurs in the vicinity of the fovea, there is irreversible loss of visual acuity.

The main purpose for the current clinical use of anti-VEGF drugs against CRVO is to suppress excessive enhancement of retinal vascular permeability; it is not to inhibit angiogenesis. VEGF enhances vascular permeability, and anti-VEGF drugs are able to mitigate the resultant macular edema. However, the beneficial effect of anti-VEGF drugs on visual acuity is not permanent³², and the need to periodically re-inject the drug increases the risk of eye infection³³. In addition, the use of large amounts of antibody increases medical expenses. For those reasons, reducing the number of injections would be beneficial from both therapeutic and financial viewpoints. Furthermore, the use of anti-VEGF drugs reportedly exacerbates retinal geographic atrophy³⁴. Moreover, because VEGF almost certainly has a physiological function in the eye, we would expect that chronic inhibition of VEGF signaling would have adverse side effects.

Hypertension, hyperlipidemia, diabetes and aging are all risk factors of CRVO. Vascular dysfunction associated with these risk factors leads to stagnation of venous blood flow within the retina, which may lead to the onset of CRVO³⁵. At present, however,

the methods available for vascular treatment are limited, and the search for novel therapeutic targets is an urgent issue.

Up to now, there have been no reports of a CRVO model in mice, except for one accidentally obtained during an attempt to generate a BRVO model³⁶. By combining intraperitoneal injection of Rose Bengal with laser irradiation, in the present study we produced a mouse model exhibiting phenotypes similar to those of clinical CRVO. To achieve an efficient photodynamic thrombotic effect, the sensitizing agent (Rose Bengal) was exposed to focused light at its peak absorption wavelength to generate oxygen singlets³⁷. Within blood vessels, the singlet oxygen induces damage to endothelial cell membranes, which likely serves as the initial stimulus for platelet adhesion and aggregation, leading to vascular occlusion. In the earlier report on the BRVO model, Rose Bengal was injected via the tail vein²⁷. However, tail vein injection is difficult in the mouse, and the procedure requires more practice than intraperitoneal injection, which is easy to perform. And because there are few failures with intraperitoneal injection, multiple samples can be handled in a single experiment.

Another advantage of the intraperitoneal injection of Rose Bengal is that the appropriate blood concentration is readily achieved. In an earlier report on central retinal artery occlusion (CRAO) model mice, Rose Bengal was injected via the tail vein³⁸, but retinal hemorrhage, which is characteristic of CRVO, was not detected. This may have been due to extensive clogging of the blood vessels. By contrast, with the lower blood concentration of Rose Bengal achieved with intraperitoneal injection, retinal arteries

could be reopened in our model. This model, therefore, shows resemblance to clinical CRVO, with retinal hemorrhage and vein dilatation with tortuosity.

A limitation of our model is that retinal artery occlusion using laser photocoagulation is accompanied by venous occlusion. In a strict sense, therefore, this model does not completely reproduce clinical human CRVO. However, using the experimental CRVO model, it was previously shown that, by itself, venous occlusion does not cause retinal hemorrhage³⁹. Retinal hemorrhage is the most characteristic phenotype of CRVO and is not observed in CRAO⁴⁰. It is caused by extravasation of blood due to venous occlusion. In our model, we were able to observe the retinal hemorrhage typical of CRVO. In past experimental studies, typical hemorrhage was observed only when both the vein and artery were occluded^{41,42}. This means that, when researchers want to produce an experimental model of CRVO, they must also transiently occlude the artery. In addition, in the clinical situation, CRVO and CRAO are sometimes observed together in the same patient⁴³. We therefore think that our model reproduces key aspects of clinical CRVO.

In our model, lack of perfusion due to blood vessel occlusion was most prominent on day 1. After that, vascular perfusion gradually improved over time, though it had not fully recovered by day 7. Because leukocyte stagnation within capillary blood vessels promotes capillary dropout⁴⁴, maintaining blood vessel density with effective blood flow and suppression of leukocyte adhesion after disease onset is considered to be important for effective treatment of CRVO. Compared with WT mice, *Adm* and *Ramp2* KO mice showed less blood flow recovery on day 7. On the other hand, vascular reperfusion after

CRVO was enhanced through exogenous ADM administration. We therefore suggest ADM could be useful for suppressing capillary dropout and improving the condition.

CRVO can also cause vision loss through secondary macular edema. Early relief of edema after the onset of CRVO is important for visual prognosis⁴⁵. Our study is the first to evaluate retinal volume in mice using OCT. In our model, as in human patients, retinal edema occurred after CRVO onset. The retinal edema gradually declined and had reached baseline levels by day 7. We also found that retinal edema was exacerbated in *Adm* KO mice, and that effect was suppressed by ADM administration.

Our quantitative real-time PCR analysis showed that expression of *Adm* and its receptor, *Calcr1* (CLR), were increased by as much as 120-fold and 6-fold, respectively, on day 3 after the CRVO. This marked upregulation of *Adm* and its receptor strongly suggests the involvement of ADM signaling in the pathogenesis of CRVO. The observed beneficial effects of exogenous ADM suggest the endogenous upregulation of *Adm* is a compensatory response to CRVO.

Damage to endothelial cells within retinal blood vessels may serve as the initial stimulus for platelet adhesion and coagulation, leading to vascular occlusion²⁷. Inflammation and oxidative stress are subsequently increased as the pathological condition progresses toward later stages⁴⁶. Consistent with that scenario, we found that expression of the coagulation factor *Serpine1* (PAI-1) was elevated at an early stage after CRVO, while inflammatory and oxidative stress markers such as *Vcam-1*, *Cd68*, *Ncf1* (p47phox), and *Ncf2* (p67phox) were elevated at a later stage. Expression of these genes was higher in *Adm* KO than WT mice, suggesting a worsening of the pathological

condition in *Adm* KO mice. Conversely, ADM administration suppressed expression of these factors, which reflects amelioration of the pathological condition. Similarly, the increase in CD68-positive macrophages and activated microglia within retina was suppressed by ADM administration. Thus, ADM appears to suppress pro-inflammatory macrophage invasion and microglial activation after CVRO.

Interestingly, we found that ADM administration also markedly suppressed the upregulation of *Kdr* (VEGFR-2) after CRVO. As VEGF signaling plays a critical role in the pathology of CRVO, which accounts for the efficacy of anti-VEGF therapy currently used to treat CRVO patients, suppression of VEGF signaling by ADM is an encouraging result from a clinical viewpoint.

Using a retinal endothelial cell line, we showed that ADM directly suppresses endothelial injury. Inflammation-, oxidative stress-related genes and *Kdr* (VEGFR-2) expression were all increased by endothelial injury, and all were suppressed by ADM administration, which is consistent with the effects of ADM administration in the CRVO model.

Figure 14 summarizes the actions and therapeutic potential of the ADM-RAMP2 system in CRVO. Virchow's triad includes the hemodynamic changes, endothelial injury and hypercoagulability that contribute to vascular thrombosis. ADM was originally identified as a vasodilating peptide and would be expected to improve blood flow in CRVO. ADM also exerts anti-coagulation effects, which may suppress the hypercoagulability in CRVO. Moreover, we showed that ADM suppresses inflammation and oxidative stress associated with CRVO, which would act coordinately to promote

endothelial injury, and also suppresses vascular hyperpermeability, which is the cause of retinal edema. Thus, its ability to break Virchow's triad makes the *Adm-Ramp2* system a promising therapeutic target for treatment of CRVO.

Anti-VEGF antibodies are already being used as standard therapy for some retinal vascular diseases, and there is no doubt about their effectiveness. However, long-term administration of anti-VEGF antibodies sometimes leads to tachyphylaxis^{4,5}. Because the biological functions of ADM and anti-VEGF antibodies are different, we think that co-administration of ADM and anti-VEGF antibodies could be an effective approach in some cases. ADM could also be useful as secondary therapy in patients who become resistant to anti-VEGF antibodies.

References

- [1] Rogers S, McIntosh RL, Cheung N, Lim L, Wang JJ, Mitchell P, Kowalski JW, Nguyen H, Wong TY, International Eye Disease C: The prevalence of retinal vein occlusion: pooled data from population studies from the United States, Europe, Asia, and Australia. *Ophthalmology* 2010, 117:313-9 e1.
- [2] O'Mahoney PR, Wong DT, Ray JG: Retinal vein occlusion and traditional risk factors for atherosclerosis. *Arch Ophthalmol* 2008, 126:692-9.
- [3] Wong TY, Scott IU: Clinical practice. Retinal-vein occlusion. *N Engl J Med* 2010, 363:2135-44.
- [4] Schaal S, Kaplan HJ, Tezel TH: Is there tachyphylaxis to intravitreal anti-vascular endothelial growth factor pharmacotherapy in age-related macular degeneration? *Ophthalmology* 2008, 115:2199-205.
- [5] Keane PA, Liakopoulos S, Ongchin SC, Heussen FM, Msutta S, Chang KT, Walsh AC, Sadda SR: Quantitative subanalysis of optical coherence tomography after treatment with ranibizumab for neovascular age-related macular degeneration. *Invest Ophthalmol Vis Sci* 2008, 49:3115-20.
- [6] Fujita Y, Mimata H, Nasu N, Nomura T, Nomura Y, Nakagawa M: Involvement of adrenomedullin induced by hypoxia in angiogenesis in human renal cell carcinoma. *Int J Urol* 2002, 9:285-95.
- [7] Wang X, Yue TL, Barone FC, White RF, Clark RK, Willette RN, Sulpizio AC, Aiyar NV, Ruffolo RR, Jr., Feuerstein GZ: Discovery of adrenomedullin in rat ischemic cortex and evidence for its role in exacerbating focal brain ischemic damage. *Proc Natl Acad Sci U S A* 1995, 92:11480-4.
- [8] Nguyen SV, Claycomb WC: Hypoxia regulates the expression of the adrenomedullin and HIF-1 genes in cultured HL-1 cardiomyocytes. *Biochem Biophys Res Commun* 1999, 265:382-6.
- [9] Shindo T, Kurihara Y, Nishimatsu H, Moriyama N, Kakoki M, Wang Y, Imai Y, Ebihara A, Kuwaki T, Ju KH, Minamino N, Kangawa K, Ishikawa T, Fukuda M, Akimoto Y, Kawakami H, Imai T, Morita H, Yazaki Y, Nagai R, Hirata Y, Kurihara H: Vascular abnormalities and elevated blood pressure in mice lacking adrenomedullin gene. *Circulation* 2001, 104:1964-71.
- [10] Iimuro S, Shindo T, Moriyama N, Amaki T, Niu P, Takeda N, Iwata H, Zhang Y, Ebihara A, Nagai R: Angiogenic effects of adrenomedullin in ischemia and tumor growth.

Circ Res 2004, 95:415-23.

[11] Brain SD, Grant AD: Vascular actions of calcitonin gene-related peptide and adrenomedullin. *Physiol Rev* 2004, 84:903-34.

[12] Kato J, Tsuruda T, Kita T, Kitamura K, Eto T: Adrenomedullin: a protective factor for blood vessels. *Arteriosclerosis, thrombosis, and vascular biology* 2005, 25:2480-7.

[13] Shimosawa T, Ogihara T, Matsui H, Asano T, Ando K, Fujita T: Deficiency of adrenomedullin induces insulin resistance by increasing oxidative stress. *Hypertension* 2003, 41:1080-5.

[14] McLatchie LM, Fraser NJ, Main MJ, Wise A, Brown J, Thompson N, Solari R, Lee MG, Foord SM: RAMPs regulate the transport and ligand specificity of the calcitonin-receptor-like receptor. *Nature* 1998, 393:333-9.

[15] Parameswaran N, Spielman WS: RAMPs: The past, present and future. *Trends Biochem Sci* 2006, 31:631-8.

[16] Ichikawa-Shindo Y, Sakurai T, Kamiyoshi A, Kawate H, Iinuma N, Yoshizawa T, Koyama T, Fukuchi J, Iimuro S, Moriyama N, Kawakami H, Murata T, Kangawa K, Nagai R, Shindo T: The GPCR modulator protein RAMP2 is essential for angiogenesis and vascular integrity. *J Clin Invest* 2008, 118:29-39.

[17] Okamura T, Ayajiki K, Kangawa K, Toda N: Mechanism of adrenomedullin-induced relaxation in isolated canine retinal arteries. *Invest Ophthalmol Vis Sci* 1997, 38:56-61.

[18] Dorner GT, Garhofer G, Huemer KH, Golestani E, Zawinka C, Schmetterer L, Wolzt M: Effects of adrenomedullin on ocular hemodynamic parameters in the choroid and the ophthalmic artery. *Investigative ophthalmology & visual science* 2003, 44:3947-51.

[19] Er H, Doganay S, Ozerol E, Yurekli M: Adrenomedullin and leptin levels in diabetic retinopathy and retinal diseases. *Ophthalmologica* 2005, 219:107-11.

[20] Ito S, Fujisawa K, Sakamoto T, Ishibashi T: Elevated adrenomedullin in the vitreous of patients with diabetic retinopathy. *Ophthalmologica* 2003, 217:53-7.

[21] Lu Y, Xu Y, Tang C: Changes in adrenomedullin in patients with proliferative diabetic retinopathy. *Current eye research* 2011, 36:1047-52.

[22] Nakamura T, Honda K, Ishikawa S, Kitamura K, Eto T, Saito T: Plasma adrenomedullin levels in patients with non-insulin dependent diabetes mellitus: close relationships with diabetic complications. *Endocrine journal* 1998, 45:241-6.

[23] Iesato Y, Toriyama Y, Sakurai T, Kamiyoshi A, Ichikawa-Shindo Y, Kawate H, Yoshizawa T, Koyama T, Uetake R, Yang L, Yamauchi A, Tanaka M, Igarashi K, Murata

- T, Shindo T: Adrenomedullin-RAMP2 system is crucially involved in retinal angiogenesis. *Am J Pathol* 2013, 182:2380-90.
- [24] Iesato Y, Yuda K, Chong KT, Tan X, Murata T, Shindo T, Yanagi Y: Adrenomedullin: A potential therapeutic target for retinochoroidal disease. *Prog Retin Eye Res* 2016, 52:112-29.
- [25] Imai A, Toriyama Y, Iesato Y, Hirabayashi K, Sakurai T, Kamiyoshi A, Ichikawa-Shindo Y, Kawate H, Tanaka M, Liu T, Xian X, Zhai L, Dai K, Tanimura K, Liu T, Cui N, Yamauchi A, Murata T, Shindo T: Adrenomedullin Suppresses Vascular Endothelial Growth Factor-Induced Vascular Hyperpermeability and Inflammation in Retinopathy. *Am J Pathol* 2017, 187:999-1015.
- [26] Khayat M, Lois N, Williams M, Stitt AW: Animal Models of Retinal Vein Occlusion. *Invest Ophthalmol Vis Sci* 2017, 58:6175-92.
- [27] Zhang H, Sonoda KH, Qiao H, Oshima T, Hisatomi T, Ishibashi T: Development of a new mouse model of branch retinal vein occlusion and retinal neovascularization. *Jpn J Ophthalmol* 2007, 51:251-7.
- [28] Paques M, Guyomard JL, Simonutti M, Roux MJ, Picaud S, Legargasson JF, Sahel JA: Panretinal, high-resolution color photography of the mouse fundus. *Invest Ophthalmol Vis Sci* 2007, 48:2769-74.
- [29] Roszer T: Understanding the Mysterious M2 Macrophage through Activation Markers and Effector Mechanisms. *Mediators Inflamm* 2015, 2015:816460.
- [30] Hayreh SS: Management of central retinal vein occlusion. *Ophthalmologica* 2003, 217:167-88.
- [31] McIntosh RL, Rogers SL, Lim L, Cheung N, Wang JJ, Mitchell P, Kowalski JW, Nguyen HP, Wong TY: Natural history of central retinal vein occlusion: an evidence-based systematic review. *Ophthalmology* 2010, 117:1113-23.e15.
- [32] Sawada O, Ohji M: Retinal Vein Occlusion. *Dev Ophthalmol* 2016, 55:147-53.
- [33] Inoue M, Kobayakawa S, Sotozono C, Komori H, Tanaka K, Suda Y, Matsushima H, Kinoshita S, Senoo T, Tochikubo T, Kadonosono K: Evaluation of the incidence of endophthalmitis after intravitreal injection of anti-vascular endothelial growth factor. *Ophthalmologica* 2011, 226:145-50.
- [34] Grunwald JE, Pistilli M, Ying GS, Maguire MG, Daniel E, Martin DF: Growth of geographic atrophy in the comparison of age-related macular degeneration treatments trials. *Ophthalmology* 2015, 122:809-16.

- [35] Kolar P: Risk factors for central and branch retinal vein occlusion: a meta-analysis of published clinical data. *J Ophthalmol* 2014, 2014:724780.
- [36] Ebnetter A, Agca C, Dysli C, Zinkernagel MS: Investigation of retinal morphology alterations using spectral domain optical coherence tomography in a mouse model of retinal branch and central retinal vein occlusion. *PLoS One* 2015, 10:e0119046.
- [37] Banks JG, Board RG, Carter J, Dodge AD: The cytotoxic and photodynamic inactivation of micro-organisms by Rose Bengal. *J Appl Bacteriol* 1985, 58:391-400.
- [38] Goldenberg-Cohen N, Dadon S, Avraham BC, Kramer M, Hasanreisoglu M, Eldar I, Weinberger D, Bahar I: Molecular and histological changes following central retinal artery occlusion in a mouse model. *Exp Eye Res* 2008, 87:327-33.
- [39] Ben-Nun J: Capillary blood flow in acute branch retinal vein occlusion. *Retina* 2001, 21:509-12.
- [40] MacDonald D: The ABCs of RVO: a review of retinal venous occlusion. *Clin Exp Optom* 2014, 97:311-23.
- [41] Hayreh SS, van Heuven WA, Hayreh MS: Experimental retinal vascular occlusion. I. Pathogenesis of central retinal vein occlusion. *Arch Ophthalmol* 1978, 96:311-23.
- [42] Wilson CA, Hatchell DL: Photodynamic retinal vascular thrombosis. Rate and duration of vascular occlusion. *Invest Ophthalmol Vis Sci* 1991, 32:2357-65.
- [43] Schmidt D: Comorbidities in combined retinal artery and vein occlusions. *Eur J Med Res* 2013, 18:27.
- [44] Miyamoto K, Ogura Y: Pathogenetic potential of leukocytes in diabetic retinopathy. *Semin Ophthalmol* 1999, 14:233-9.
- [45] Thach AB, Yau L, Hoang C, Tuomi L: Time to clinically significant visual acuity gains after ranibizumab treatment for retinal vein occlusion: BRAVO and CRUISE trials. *Ophthalmology* 2014, 121:1059-66.
- [46] Noma H, Mimura T, Eguchi S: Association of inflammatory factors with macular edema in branch retinal vein occlusion. *JAMA Ophthalmol* 2013, 131:160-5.

Figure legends

Figure 1

Evaluation of retinal hemorrhage in the CRVO model.

A: Topical endoscopy fundus imaging showing the ocular fundus of untreated and CRVO-treated mice (day 7). In the CRVO-treated mice, note the retinal hemorrhage and venous dilatation with tortuousness resembling clinical CRVO. **B:** Retinal flat-mount images of untreated and CRVO-treated mice (day 7). Retinal hemorrhage is prominent in the CRVO-treated mice.

Figure 2

Evaluation of vascular perfusion in the CRVO model.

A: Representative fluorescein angiography (FA) images from untreated control and CRVO-treated mice (days 1, 3 and 7) (upper panels). FA images were analyzed using AngioTool software (lower panels). Blood vessels are depicted in red, and vascular branch points are depicted in blue. **B:** Percent vascular areas in FA images quantified using AngioTool. Bars are means \pm SEM. $n = 6$ in each group. $*p < 0.05$, $****p < 0.0001$ (Dunnett's test). **C:** FITC-perfused retinal flat-mount images from untreated control mice and CRVO-treated mice (day 7) (upper panels). FITC-perfused retinal flat-mount images were analyzed using AngioTool (lower panels). Blood vessels are depicted in red, and vascular branches are depicted in blue. **D:** Percent vascular area in FITC-perfused retinal flat-mount images on day 7 quantified using AngioTool. Bars are means \pm SEM.

untreated: n = 5, CRVO: n = 6. **p<0.01 (Unpaired t-test).

Figure 3

Evaluation of retinal volume in the CRVO model using OCT-imaging.

A: Representative OCT color mapping around the optic disc. The degree of retinal edema is shown from yellow to red, while retinal atrophy is shown in blue. **B:** B-scan of OCT showing cross sections of retina between the internal limiting membrane (ILM) and the basement membrane (BM) (red lines) around the optic disc. Green bars represent the center lines of retina. Scale bars = 200 μ m. **C:** Retinal volume in a 6-mm diameter area around the optic disc calculated using the OCT algorithm. Data are expressed as means \pm SEM. n = 4~6. *p<0.05, ***p<0.001, ****p<0.0001 (Dunnett's test).

Figure 4

Evaluation of retinal blood flow based on OCT angiography and histological changes in the CRVO model.

A: OCT angiography with or without CRVO treatment. Between the main retinal blood vessels radiating from the optic disc, smaller capillaries were well visualized in untreated mice. The smaller capillaries became invisible by day 7. The main retinal blood vessels were shrunken on Day 21. Green bars represent the center lines of retina. Scale bars = 200 μ m. **B:** B-scan of OCT showing cross sections of retina between the internal limiting membrane (ILM) and the basement membrane (BM) (red lines) around

the optic disc. Retinal layers showing blood flow signals (yellow) are enlarged in the lower panels. In untreated mice, blood flow signals were detected in both the superficial and deep layers, which respectively represent blood flow of main retinal blood vessels and smaller capillaries. The blood flow in smaller capillaries in the deep layers was undetectable on days 7 and 21. **C:** Retinal sections with HE staining. Retinal edema was prominent from day 1 to 7, especially at the inner layer of the retina. On day 7, decidualization of the cells in inner nuclear layer and abnormal cavity formation within the choroid were noticeable (arrows in day 7). On day 21, the inner layers of the retina were undetectable; only the outer layers of the retina were detectable. RNFL, retinal nerve fiber layer; GCL, ganglion cell layer; IPL, inner plexiform layer; INL, inner nuclear layer; OPL, outer plexiform layer; ONL, outer nuclear layer; RPE, retinal pigment epithelium. Scale bars = 100 μm .

Figure 5

Evaluation of macrophages and microglia in retinal flat-mounts.

A, Comparison of FITC-perfused and isolectin B4-stained retinal flat-mounts on day 7 after CRVO. The distribution of FITC-positive and isolectin B4-positive areas are strikingly different. With FITC-perfusion, nonperfused areas were not clearly seen, whereas isolectin B4-stained areas were more likely to be detected in nonperfused areas. Scale bars = 100 μm . **B,** Comparison of isolectin B4 staining and F4/80 immunostaining of retinal flat-mounts on day 7 after CRVO. Isolectin B4 staining was detected on small round structures with dendrites, which were clearly different from the vascular branch

structures (left panel). These structures were also positive for the macrophage marker F4/80 (middle panel), showing that macrophage numbers were increased in nonperfused areas after CRVO. Scale bars = 50 μ m. **C:** CD68 immunostaining of retinal flat-mounts after CRVO. CD68-positive macrophages and activated microglia increased over time from day 1 to day 7. Scale bars = 100 μ m. **D:** Percent CD68- or CD206-positive cells among isolectin B4-positive cells in retinal flat-mounts after CRVO (Isolectin B4-positive vessels were excluded from the calculation.). CD68-positive cells were rarely observed before CRVO, but increased after CRVO. Data are expressed as means \pm SEM. n = 5 in each group.

Figure 6

Comprehensive gene expression analysis in retinas with and without CRVO.

A, B: Clustergram showing the results of real-time PCR array analysis of angiogenesis-related (**A**) and endothelial cell-related (**B**) molecules in mouse retinas with and without CRVO treatment. Each column shows the results from one mouse. Red and green colors represent higher and lower gene expression, respectively. (Gene names from top to bottom in **A**; *Smad5, Cxcl5, Erbb2, Coll8a1, Tgfa, Tgfb1, Itgav, Mmp2, Flt1, Pecam1, Vegfa, Efna1, Cdh5, Kdr, Mmp14, Thbs1, B2m, Pdgfa, Cxcl2, Ccl2, Cxcl1, Fgf2, Itgb3, Fn1, Plau, Pgf, Serpine1, Timp1, F3, Slpr1, Actb, Angpt2, Hsp90ab1, Mdk, Nrp1, Tgfb2, Angpt1, Eng, Timp2, Gusb, Fgfr3, Vegfc, Akt1, Epas1, Hif1a, Mapk14, Efnb2, Jag1, Tnfsf12, Tek, Nos3, Adgrb1, Vegfb, Tgfb3, Lect1, Gapdh, Nrp2, Fgf1, Mmp9, Hgf, Serpinf1, Col4a3, Igf1, Tgfbr1, RTC, RTC, RTC, Ptk2, PPC, PPC, PPC, Egf, Ephb4, Tbx1,*

Tie1, Ctgf, Sphk1, Ccl11, Il1b, Edn1, Ptgs1, Csf3, Tymp, Figf, F2, Mmp19, MGDC, Anpep, Il6, Ang, Thbs2, Tnf, Lep, Plg, Fgf6, Ifng. Gene names from top to bottom in **B**; *Plg, I111, Sele, Thbs1, Il1b, Itgb3, Edn2, Plat, Tgfb1, Itgb1, Itgav, Mmp2, Pgf, Procr, Plau, B2m, Fgf2, Pf4, Serpine, Timp1, Fn1, Anxa5, Ptgs2, Col18a1, F3, F2r11, Actb, Icam1, Cxcl2, Fas, Ccl2, Cxcl1, Sell, Vcam1, Selp, Agtr1a, Il17, Tnfsf10, Kit, RTC, RTC, RTC, PPC, PPC, PPC, Thbd, Cxcr5, Npr1, Il6, Nppb, Sod1, Bcl2, Cradd, Angpt1, Eng, Agt, Apoe, Ednra, F2r, Fgf1, Cx3c11, Mmp9, Ocln, Hif1a, Ptgis, Itga5, MGDC, Selplg, Nos3, Tek, Gapdh, Ace, Mmp1a, Il13, Tfpi, Ccl5, Hsp90ab1, Tymp, Gusb, Fas1, Vwf, Vegfa, Cdh5, Flt1, Pdgfra, Casp3, Bcl2l1, Cflar, Adam17, Bax, Tnf, Cav1, Edn1, Pecam1, Casp1, Kdr.)*

C: Dot plot showing the results of the real-time PCR array analysis. The horizontal axis shows the fold change ($\log_2(\text{fold change})$), and the vertical axis shows the p-value ($-\log_{10}(\text{p-value})$). Two dotted lines indicate the distribution of unchanged genes. In CRVO-treated mice, expression of chemokines, growth factors and coagulation factors was upregulated as compared to untreated mice (Shown in red dots). Some angiogenic factors were downregulated in the vascular occlusion group (Shown in green dots).

Figure 7

Quantitative real-time PCR analysis of retinas with or without CRVO.

A: Relative expression of coagulation-, inflammation-, and oxidative stress-related genes in the retinas of untreated mice and on days 1, 3 and 7 after CRVO. The mean of the

control group without CRVO treatment (Ctrl) was assigned a value of 1. Data are expressed as means \pm SEM. n = 4 in each group. *p<0.05 (Dunnett's test). **B**, Relative expression of *Adm* and its related genes in retinas of untreated mice and on days 1, 3 and 7 after CRVO. Data are expressed as means \pm SEM. n = 4 in each group. *p<0.05, ***p<0.001 (Dunnett's test).

Figure 8

***Adm* and *Ramp2* KO mice show reduced vascular perfusion after CRVO.**

A: FA images analyzed using AngioTool software in WT, *Adm* KO and *Ramp2* KO mice after CRVO treatment (days 1, 3 and 7). Blood vessels are depicted in red, and vascular branch points are depicted in blue. **B**: Percent vascular area in FA images quantified using AngioTool. Bars are means \pm SEM. n = 5~8. **C**: FITC-perfused retinal flat-mount images analyzed using AngioTool. Blood vessels are depicted in red, and vascular branch points are depicted in blue. **D**, Percent vascular area in FITC-perfused retinal flat-mounts quantified using AngioTool. Bars are means \pm SEM. n = 5~7. *p<0.05 (Dunnett's test).

Figure 9

Gene expression and macrophage distribution in the retinas of *Adm* KO mice.

A, Quantitative real-time PCR analysis showing the relative expression levels of the indicated genes in the retinas of *Adm* KO and WT mice. The mean in WT mice was assigned a value of 1. Bars are means \pm SEM. n = 4 in each group. *p<0.05, **p<0.01

(Unpaired t-test). **B**, Percent CD68- or CD206-positive cells among isolectin B4-positive cells in retinal flat-mounts after CRVO. Bars are means \pm SEM. n = 8~10 in each group. Percentages of CD68-positive macrophages and activated microglia were increased while CD206-positive resident microglia were decreased in *Adm* KO as compared to WT mice.

Figure 10

ADM administration improves vascular perfusion after CRVO.

A: FA images of retinas analyzed using AngioTool software in control WT mice (Ctrl) and WT mice administered ADM (ADM pump) on the indicated days after CRVO.

Blood vessels are depicted in red, and vascular branch points are depicted in blue. **B**:

Percent vascular area in the FA images quantified using AngioTool software. Bars are means \pm SEM. n = 4~9. **C**: FITC-perfused retinal flat-mounts analyzed using

AngioTool. Blood vessels are depicted in red, and vascular branch points are depicted in blue. **D**: Percent vascular area in FITC-perfused retinal flat-mounts quantified using

AngioTool. Bars are means \pm SEM. n = 5 in each group. **p<0.01 (Unpaired t-test).

ADM administration improved vascular perfusion.

Figure 11

Gene expression and macrophage distribution in the retinas of mice administered ADM.

A: Quantitative real-time PCR analysis showing the relative expression of the indicated

genes in the retinas of control WT mice (Ctrl) and WT mice administered ADM (ADM pump). The mean of the Ctrl group was assigned a value of 1. Bars are means \pm SEM. n = 4 in each group. * $p < 0.05$, ** $p < 0.01$ (Unpaired t-test). **B:** Percent CD68- or CD206-positive cells among isolectin B4-positive cells in retinal flat-mounts after CRVO. Bars are means \pm SEM. n = 5 in each group. Percentages of CD68-positive macrophages and activated microglia were decreased while CD206-positive resident microglia were increased by intravitreal injection of ADM.

Figure 12

Retinal damage was enhanced in *Adm* KO and suppressed by ADM-administration.

HE-staining (left panels) and p67phox-immunostaining (right panels) in cross sections showing the retinal layers on day 7 after CRVO. Scale bars = 100 μ m. Disruption of the internal retinal layer was exacerbated in *Adm* KO mice, and suppressed in the mice administered ADM (ADM pump). *Adm* KO mice also showed elevated p67phox expression, indicating higher oxidative stress.

Figure 13

ADM directly suppresses retinal endothelial injury.

Quantitative real-time PCR analysis showing relative expression of the indicted genes in TR-iBRB cells, an immortalized retinal capillary endothelial cell line. The mean of the control group (Ctrl) was assigned a value of 1. Endothelial injury was induced by

exposing the cells to TNF- α (20 ng/ml) for 24 h in the presence or absence of ADM (10^{-7} or 10^{-9} M). Data are expressed as means \pm SEM. n = 5~7. *p<0.05, **p<0.01, ****p<0.0001 (Dunnett's test).

Figure 14

Summary of the actions and therapeutic potential of the ADM-RAMP2 system in CRVO.

Virchow's triad describes the three elements (hemodynamic changes, endothelial injury and hypercoagulability) that contribute to vascular thrombosis. ADM was originally identified as a vasodilating peptide and would be expected to improve reperfusion of vessels in which blood flow was interrupted by CRVO. ADM also exerts anti-coagulation effects, which may suppress the hypercoagulability in CRVO. In addition, ADM suppresses inflammation and oxidative stress associated with CRVO, which coordinately promote endothelial injury. Finally, ADM suppresses vascular hyperpermeability, which is the cause of retinal edema. ADM appears to break Virchow's triad, making it a promising therapeutic target for the treatment of CRVO.

Supplementary Figure legends

Supplementary Figure 1

Evaluation of retinal layer in CRVO model using OCT equipment for smaller experimental animals.

Representative OCT images of the retina obtained using equipment for smaller experimental animals (Envisu R-Class OCT, Leica Microsystems) without and with CRVO (days 1 and 20).

Supplementary Figure 2

Evaluation of retinal thickness in CRVO model using OCT equipment for smaller experimental animals.

Measurement of retinal thickness. Data are expressed as means \pm SEM. n = 10~22 in each group. *p<0.05, **p<0.01, ****p<0.0001 (Dunnett's test). The retinal edema was most prominent on day 1 after CRVO, but it declined to baseline by day 7. Retinal atrophy was then observed on day 20.

Supplementary Figure 3

Serum ADM levels in ADM KO and ADM-administered mice.

Serum ADM levels were measured using Mouse ADM ELIZA Kit (MyBioSource, CA). Data are expressed as means \pm SEM. n = 5~6 in each group. In *Adm* KO mice, serum ADM was reduced to 70% of the level in wild-type mice. In ADM-administered mice,

serum ADM was 50% higher than in wild-type mice.

Supplementary Figure 4

Comprehensive gene expression analysis in retinas of control and ADM-administered mice with CRVO.

Dot plot showing the results of a real-time PCR array analysis (RT² Profiler PCR Array angiogenesis-related molecules (QIAGEN)). The horizontal axis shows the fold change ($\log_2(\text{fold change})$), and the vertical axis shows the p-value ($-\log_{10}(\text{p-value})$). Two dotted lines indicate the distribution of unchanged genes. Red dots indicate genes upregulated in ADM-administered mice as compared to control mice. Green dots indicate downregulated genes.

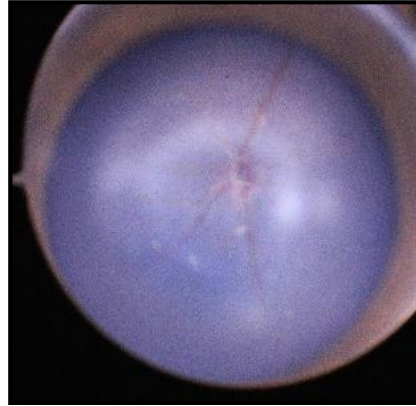
Table1 Primers Used for real-time PCR

m <i>Calcr1</i> (CLR) Forward	5'-AGGCGTTTACCTGCACACACT-3'
m <i>Calcr1</i> (CLR) Reverse	5'-CAGGAAGCAGAGGAAACCCC-3'
m <i>Calcr1</i> (CLR) Probe	5'-ATCGTGGTGGCTGTGTTTGCGGAG-3'
m <i>Ramp1</i> Forward	5'-GCACTGGTGGTCTGGAGGA-3'
m <i>Ramp1</i> Reverse	5'-CCCTCATCACCTGGGATACCT-3'
m <i>Ramp1</i> Probe	5'-CAAGCGCACAGAGGGCATCGTG-3'
m <i>Ramp2</i> Forward	5'-GCAGCCCACCTTCTCTGATC-3'
m <i>Ramp2</i> Reverse	5'- AACGGGATGAGGCAGATGG-3'
m <i>Ramp2</i> Probe	5'- CCCAGAGGATGTGCTCCTGGCCAT -3'
m <i>Ramp3</i> Forward	5'-TGCAACGAGACAGGGATGC-3'
m <i>Ramp3</i> Reverse	5'-GCATCATGTCAGCGAAGGC-3'
m <i>Ramp3</i> Probe	5'-AGAGGCTGCCTCGCTGTGGGAA-3'
TaqMan m <i>Adm</i> Forward	5'-CTACCGCCAGAGCATGAACC-3'
TaqMan m <i>Adm</i> Reverse	5'-GAAATGTGCAGGTCCCGAA-3'
TaqMan m <i>Adm</i> Probe	5'-CCCGCAGCAATGGATGCCG-3'
SYBR m <i>Adm</i> Forward	5'-GGACACTGCAGGGCCAGAT-3'
SYBR m <i>Adm</i> Reverse	5'-GTAGTTCCTCTTCCCACGACTTA-3'
m <i>Serpine1</i> (PAI-1) Forward	5'-ACCAAGAGCAGCTCTCTGTAGCA-3'
m <i>Serpine1</i> (PAI-1) Reverse	5'-CTTGGCCCATGAAGAGGATTGTCT-3'
m <i>Vcam-1</i> Forward	5'-CCCTGAATACAAAACGATCGC-3'
m <i>Vcam-1</i> Reverse	5'-CAGCCCGTAGTGCTGCAAG-3'
m <i>Cd68</i> Forward	5'-TGGCGGTGGAATACAATGTG-3'
m <i>Cd68</i> Reverse	5'-GAGATGAATTCTGCGCCATGA-3'

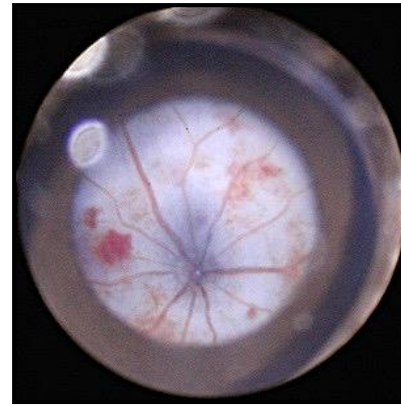
m <i>Ncf1</i> (p47phox) Forward	5'-ATCCTATCTGGAGCCCCTTGA-3'
m <i>Ncf1</i> (p47phox) Reverse	5'-CACCTGCGTAGTTGGGATCC-3'
m <i>Ncf2</i> (p67phox) Forward	5'-CAGACCCAAAACCCAGAAA-3'
m <i>Ncf2</i> (p67phox) Reverse	5'-AAAGCCAAACAATACGCGGT-3'
m <i>Nos3</i> (eNOS) Forward	5'-AGGCACTGCTGAGCCGAGT-3'
m <i>Nos3</i> (eNOS) Reverse	5'-TTCTCCAGTTGTTCCACAGCC-3'
m <i>Tek</i> (Tie-2) Forward	5'-GGAACCTGACCTCGGTGCTA-3'
m <i>Tek</i> (Tie-2) Reverse	5'-CTGCGCCTTGGTGTGACT-3'
m <i>Angpt1</i> Forward	5'-CATGGGCAATGTGCCTACAC-3'
m <i>Angpt1</i> Reverse	5'-TCGCACTCTCACGGCAGTT-3'
m <i>Tnf-α</i> Forward	5'-ACGGCATGGATCTCAAAGAC-3'
m <i>Tnf-α</i> Reverse	5'-AGATAGCAAATCGGCTGACG-3'
m <i>Kdr</i> (VEGFR2) Forward	5'-ACTGCAGTGATTGCCATGTTCT-3'
m <i>Kdr</i> (VEGFR2) Reverse	5'-TCATTGGCCCGCTTAAGG-3'
r <i>Gapdh</i> Forward	5'-AGACAGCCGCATCTTCTTGT-3'
r <i>Gapdh</i> Reverse	5'-CTTGCCGTGGGTAGAGTCAT-3'
r <i>Vcam -1</i> Forward	5'-GGGATTAATGAGGCTGGAAT-3'
r <i>Vcam -1</i> Reverse	5'-TGTCTCCTGTCTTGGCTTTC-3'
r <i>Ccl2</i> (MCP-1) Forward	5'-GAAAATCACAAGCAGCCAGT-3'
r <i>Ccl2</i> (MCP-1) Reverse	5'-GGGGAAGGTCAGAGGAAATA-3'
r <i>Ncf1</i> (p47phox) Forward	5'-TGCACAGAGAGCACCAAGAG-3'
r <i>Ncf1</i> (p47phox) Reverse	5'-GGTAGGAGCCTCTGACCTGA-3'
r <i>Ncf2</i> (p67phox) Forward	5'-CCCCACTCGAGGATTTGCTT-3'
r <i>Ncf2</i> (p67phox) Reverse	5'-TCGCTGGAAGTAAGCCACTG-3'
r <i>Kdr</i> (VEGFR2) Forward	5'-GGGTTTTGTCAAGTGGCGAC-3'

r <i>Kdr</i> (VEGFR2) Reverse	5'-ATCACGTGGCCACAAAGCTA-3'
r <i>Cd68</i> Forward	5'-ACAGTTTCTCCCACCACAAA-3'
r <i>Cd68</i> Reverse	5'-CCTGGGTCAGGTACAAGATG-3'

A Day7
No treatment



CRVO treatment



B Day7
No treatment



CRVO treatment

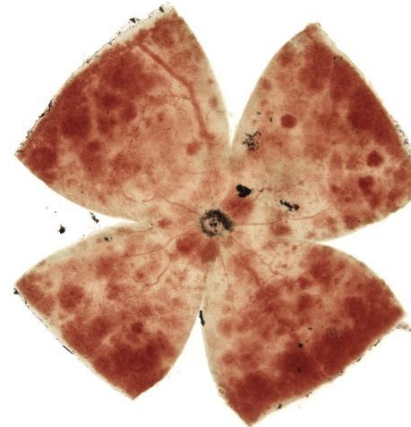


Figure 1

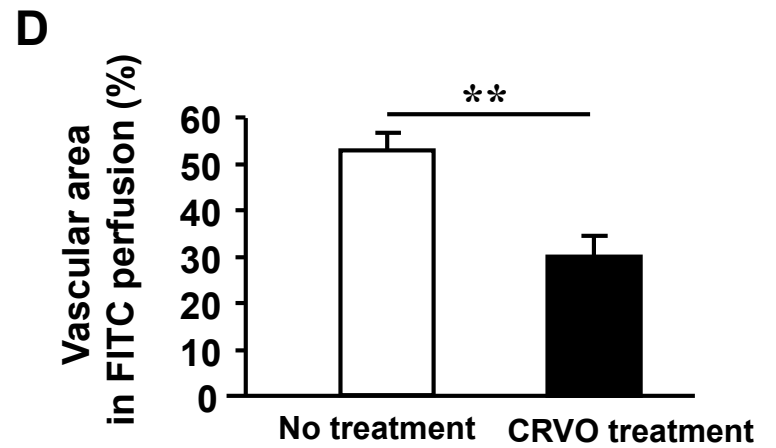
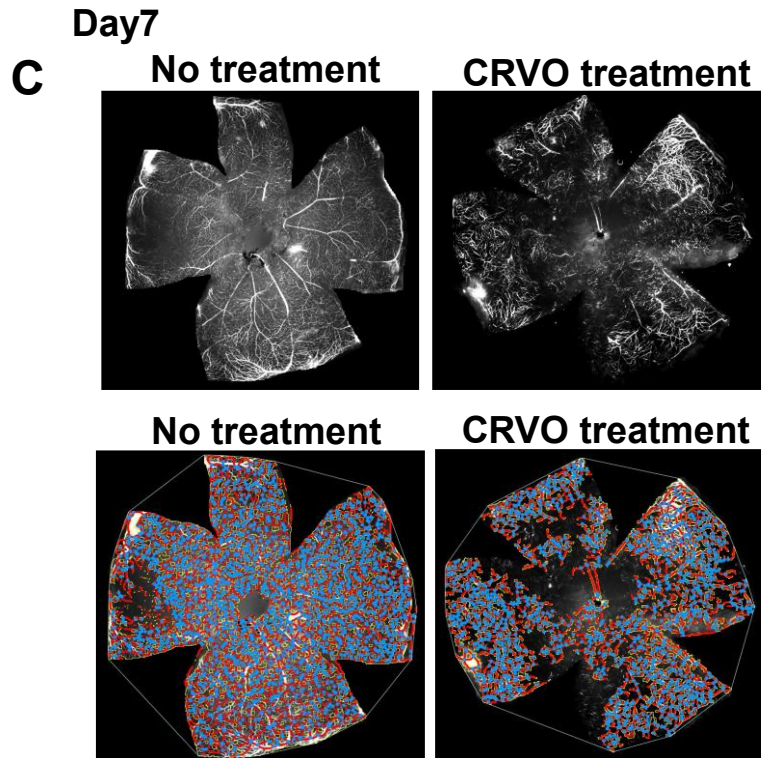
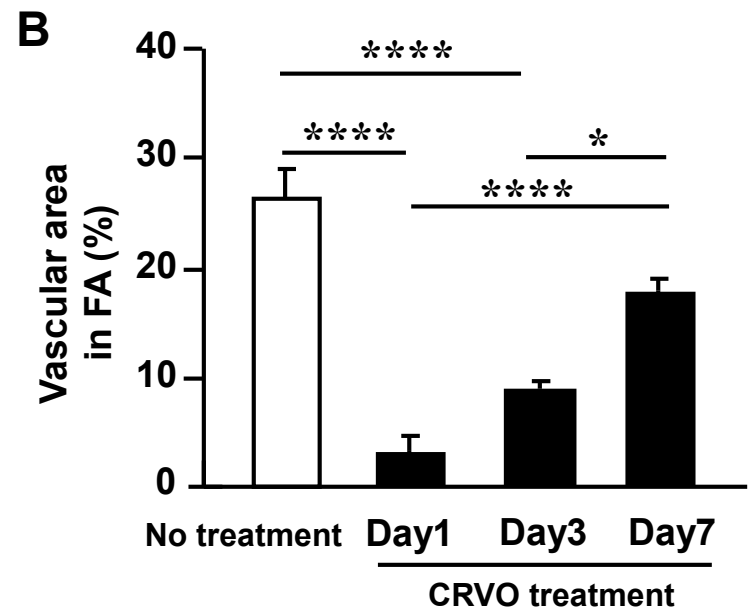
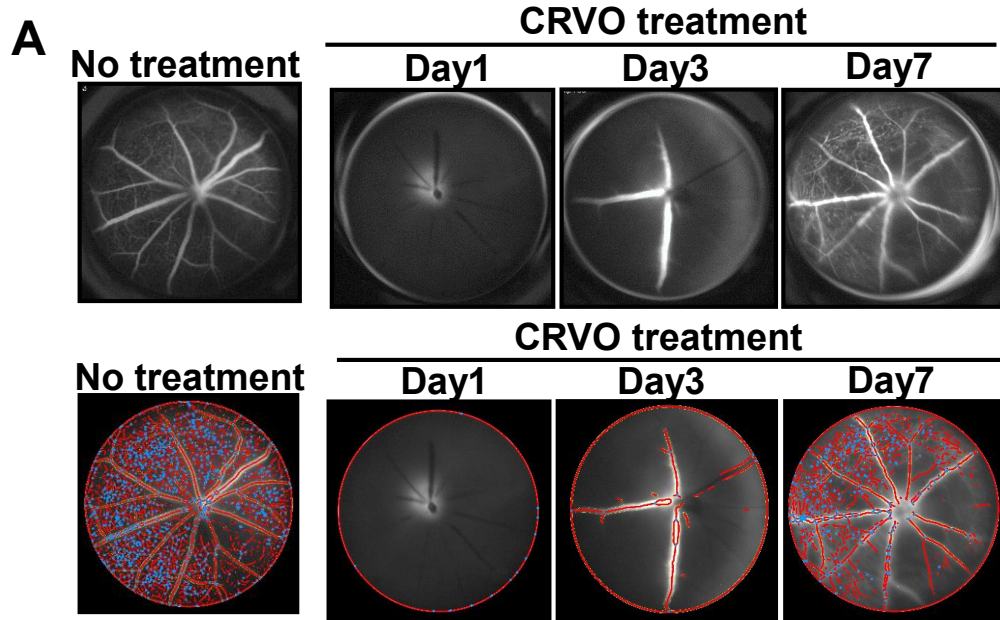
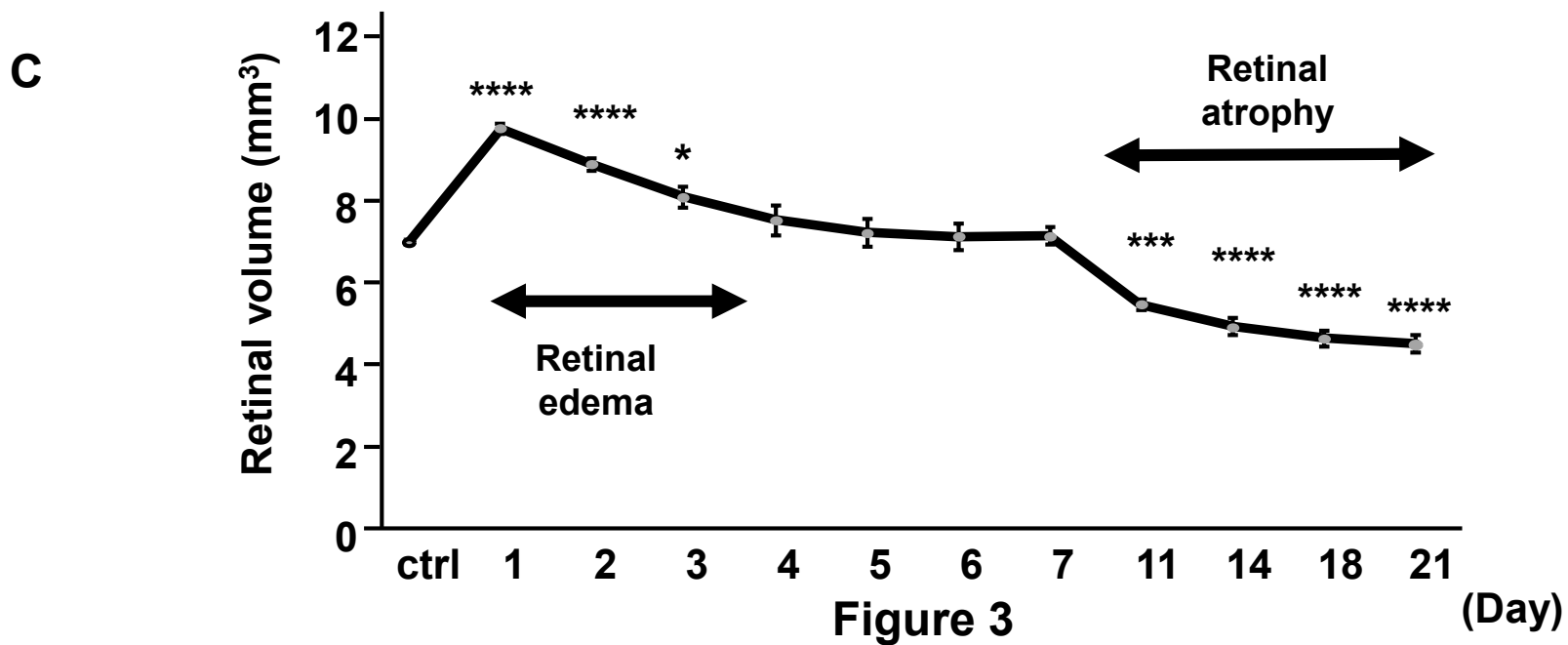
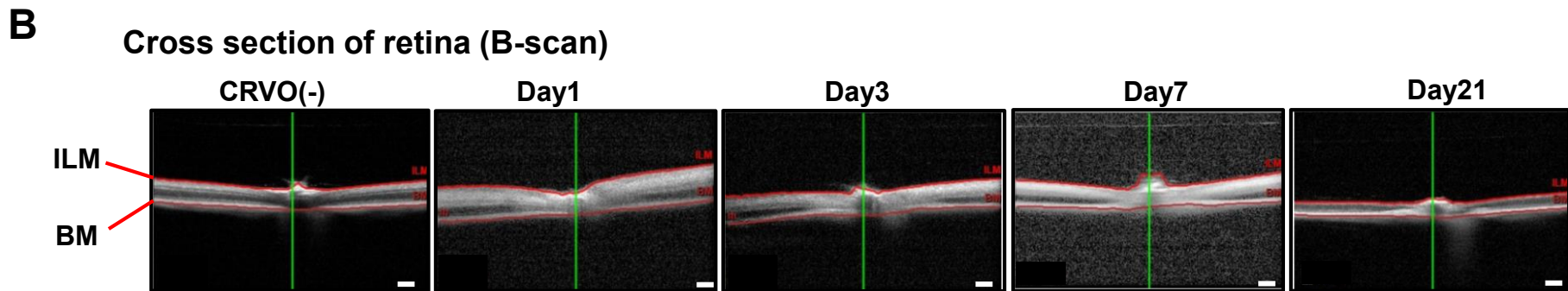
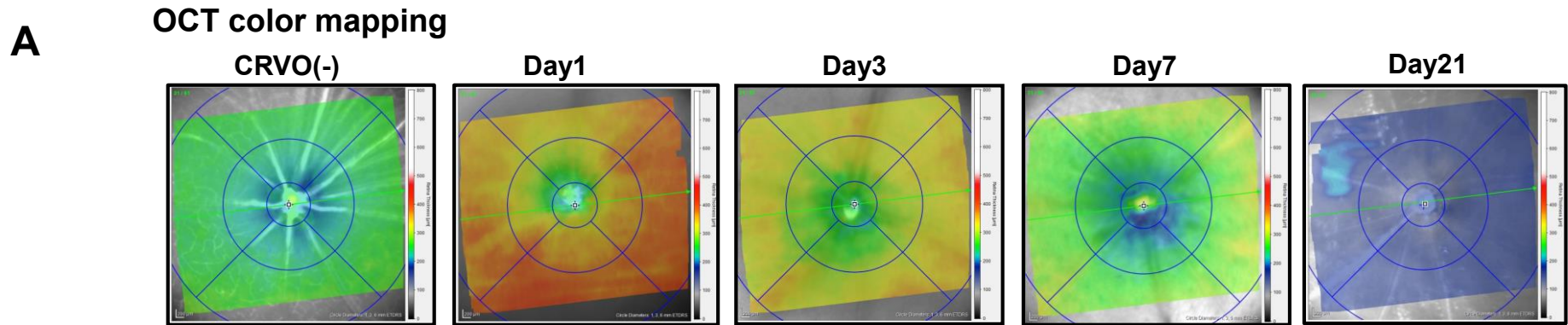
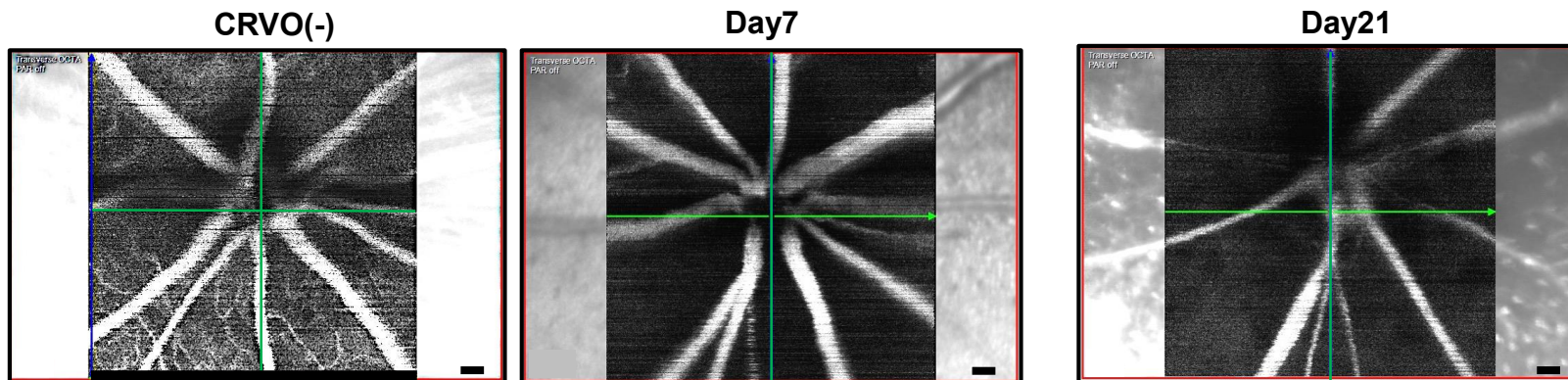


Figure 2



OCT angiography

A



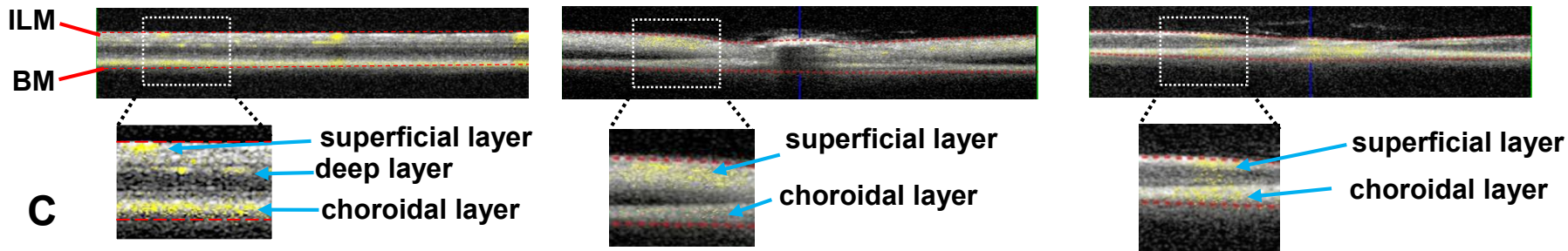
B

OCT angiography (B scan)

CRVO(-)

Day7

Day21



C

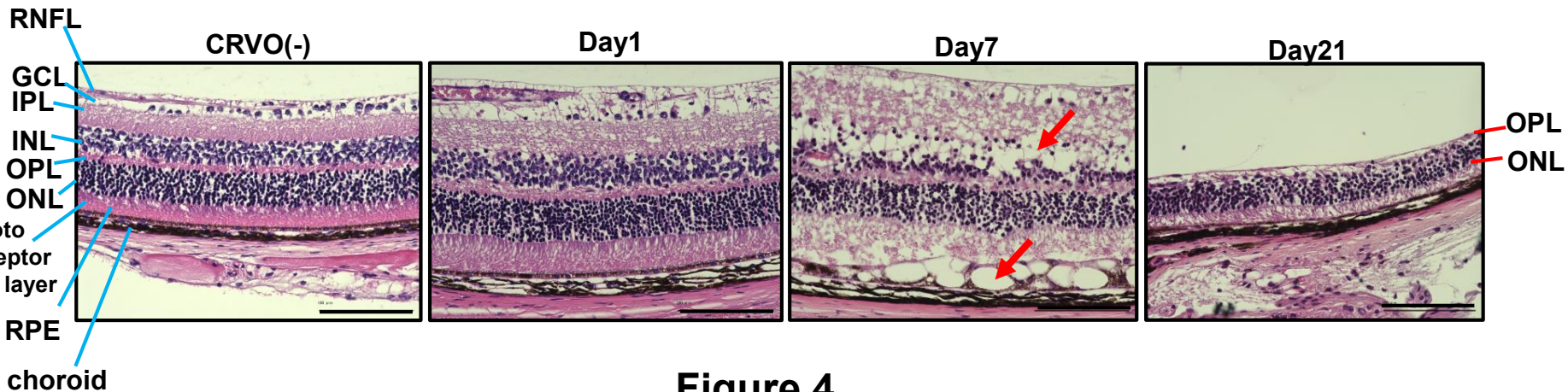
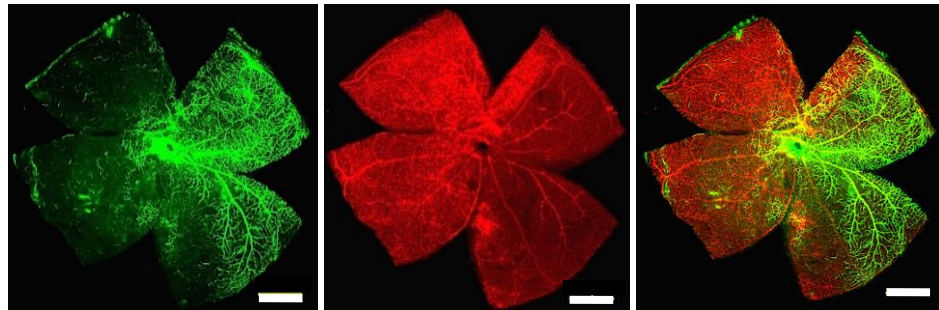


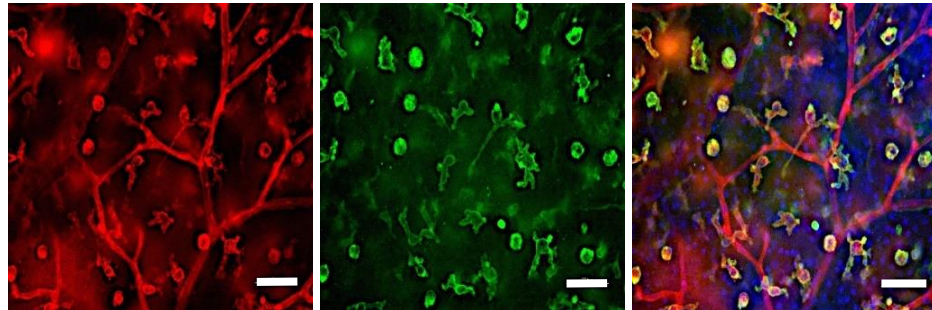
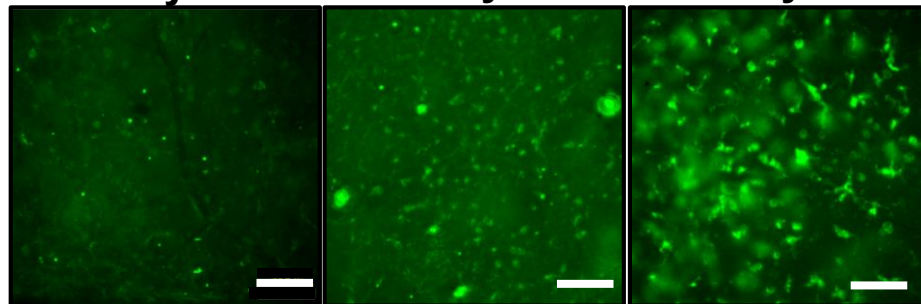
Figure 4

A**Day 7****FITC****Isolectin B4****Merge**

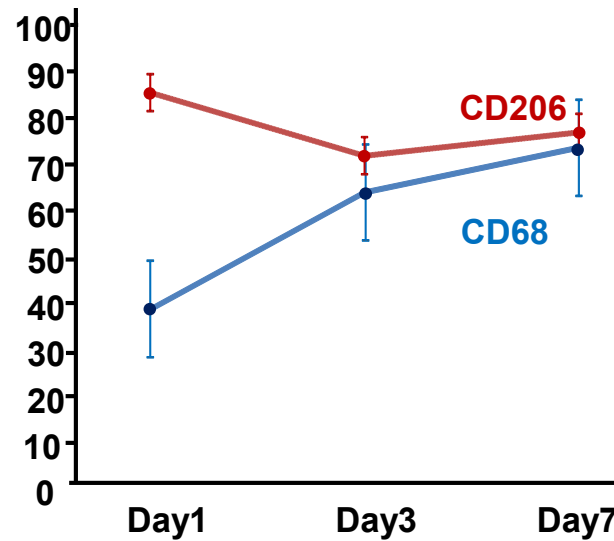
FITC, Isolectin B4

**B****Day 7****Isolectin B4****F4/80****Merge**

Isolectin B4, F4/80, DAPI

**C****CD68 immunostain****Day1****Day3****Day7****D**

CD68 or CD206-positive cells
/ isolectin B4-positive cells (%)

**Figure 5**

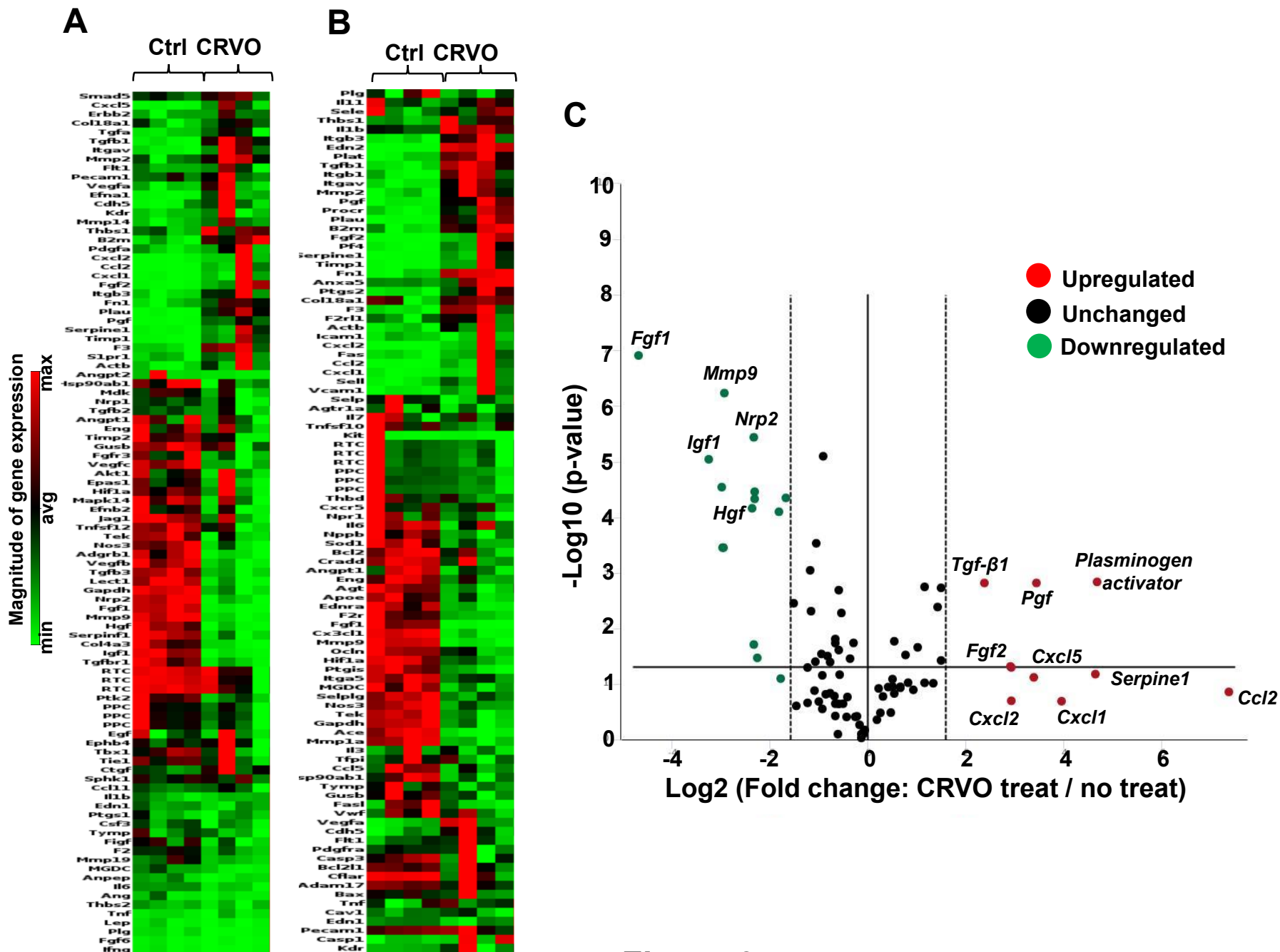


Figure 6

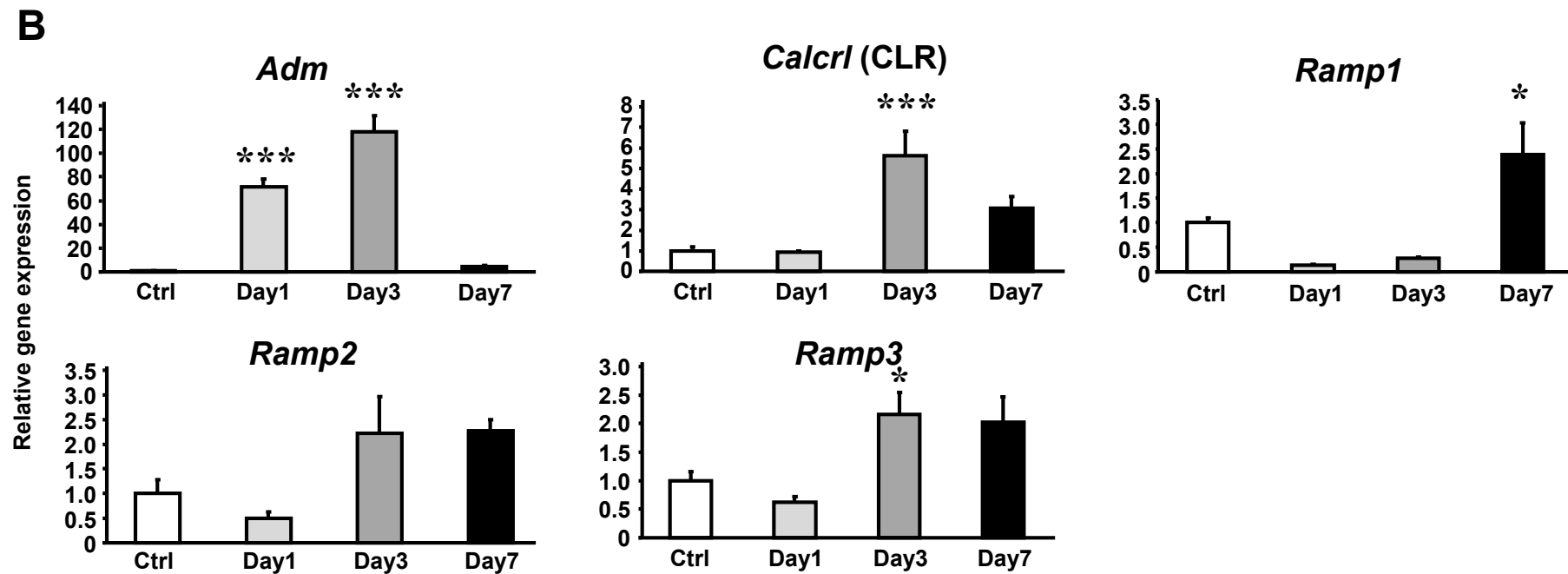
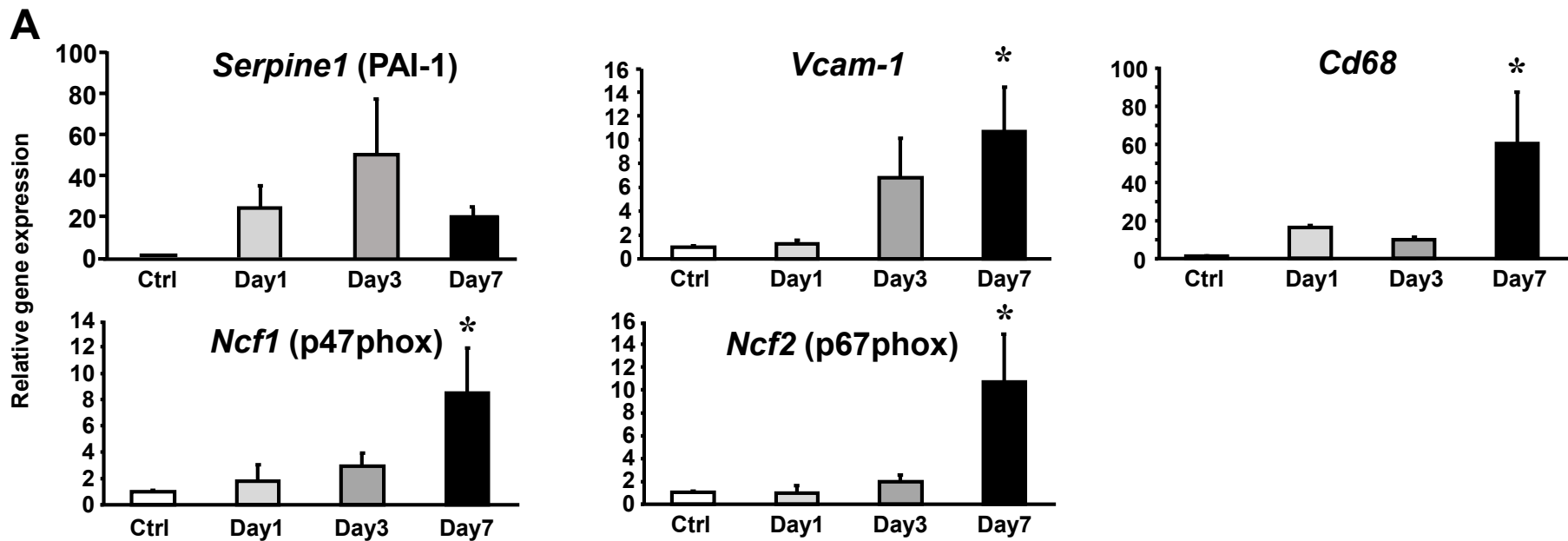


Figure 7

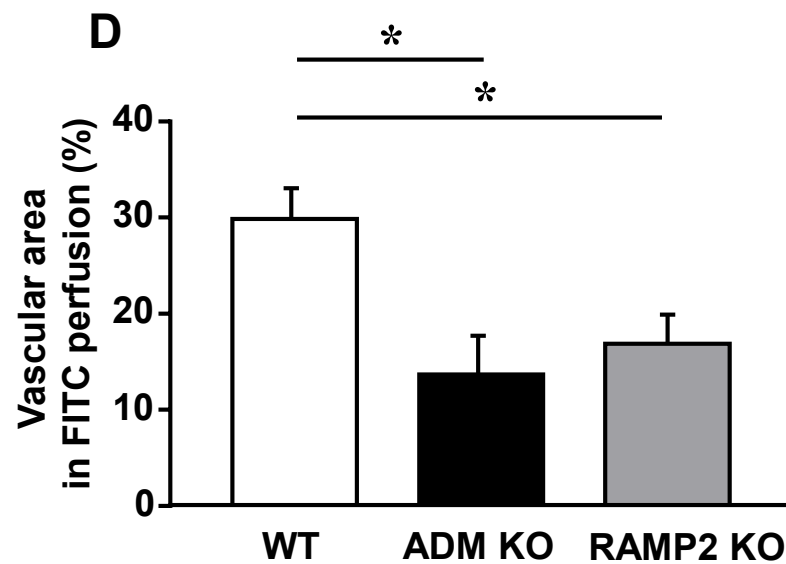
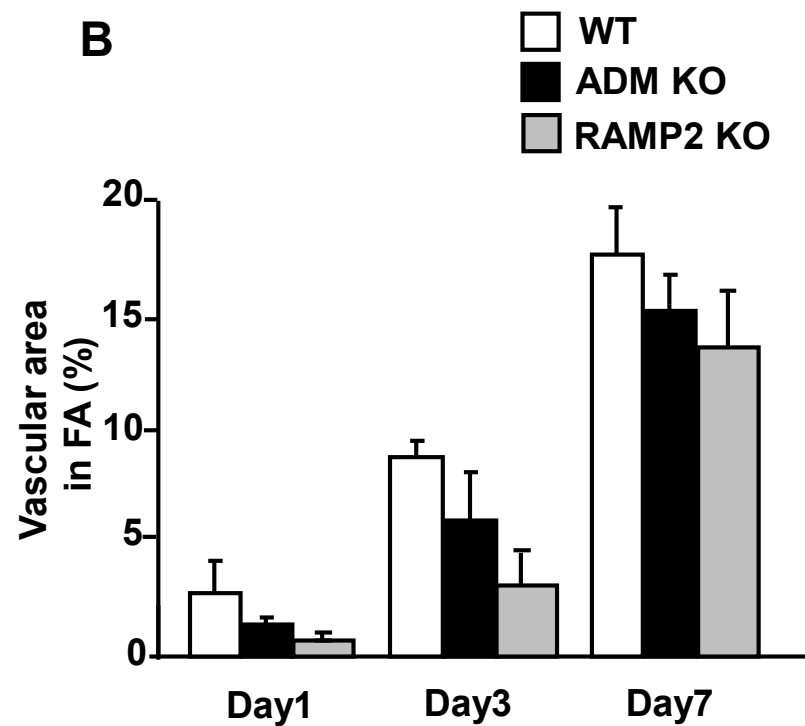
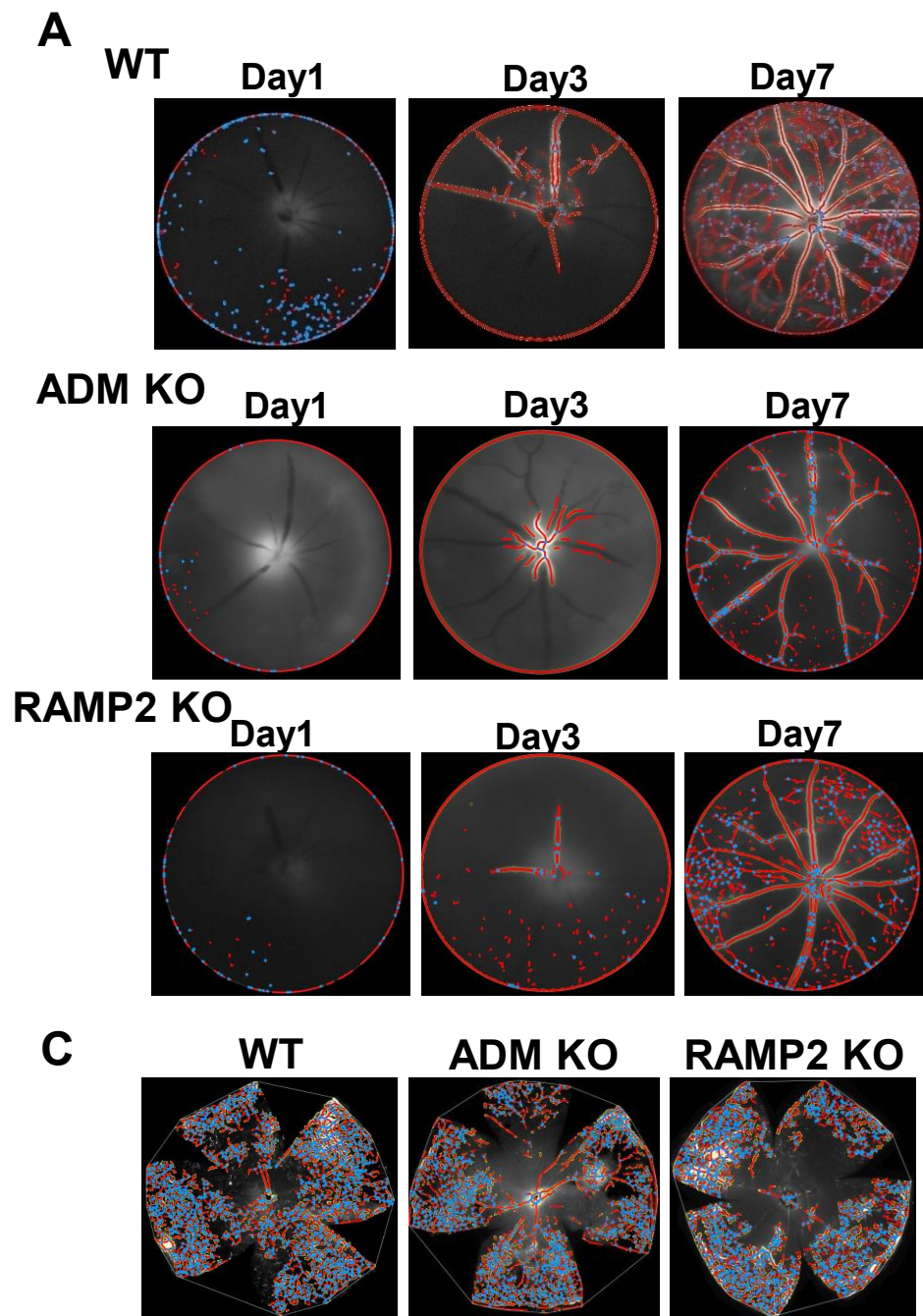
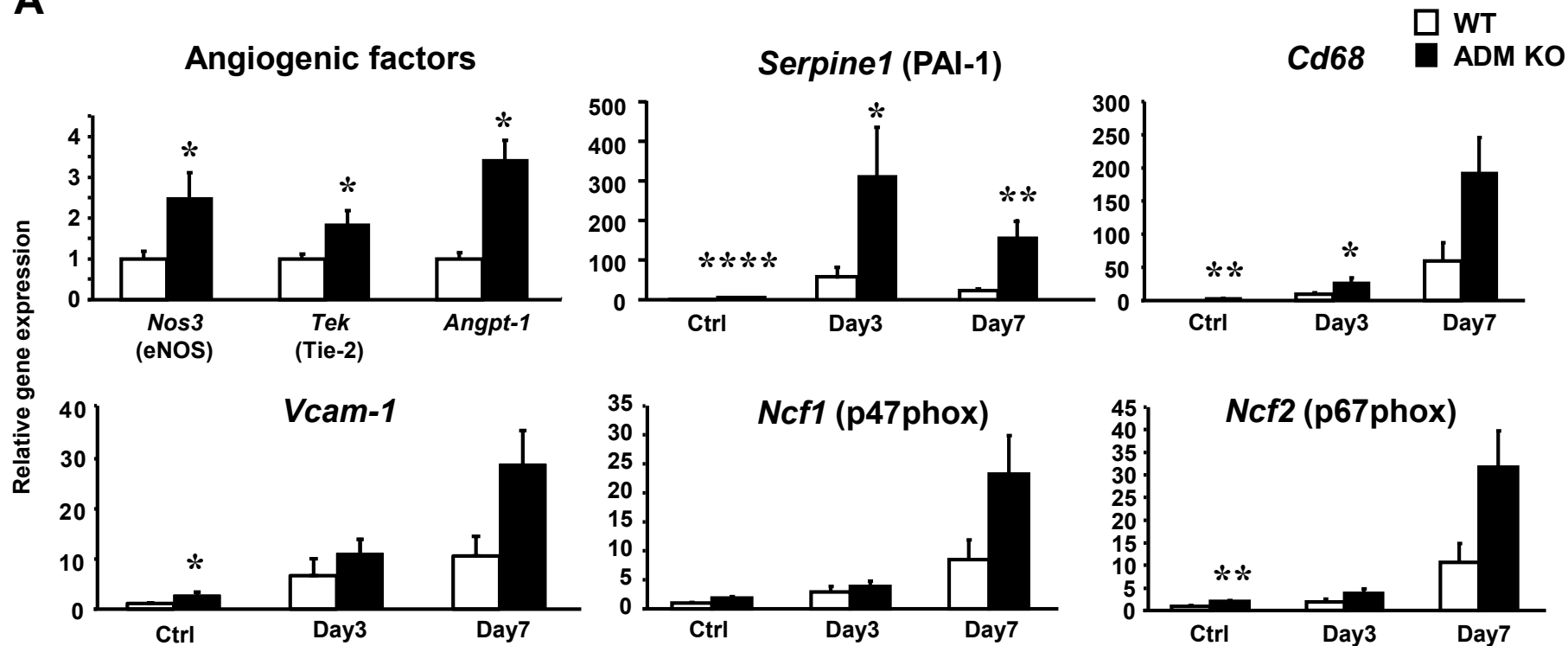
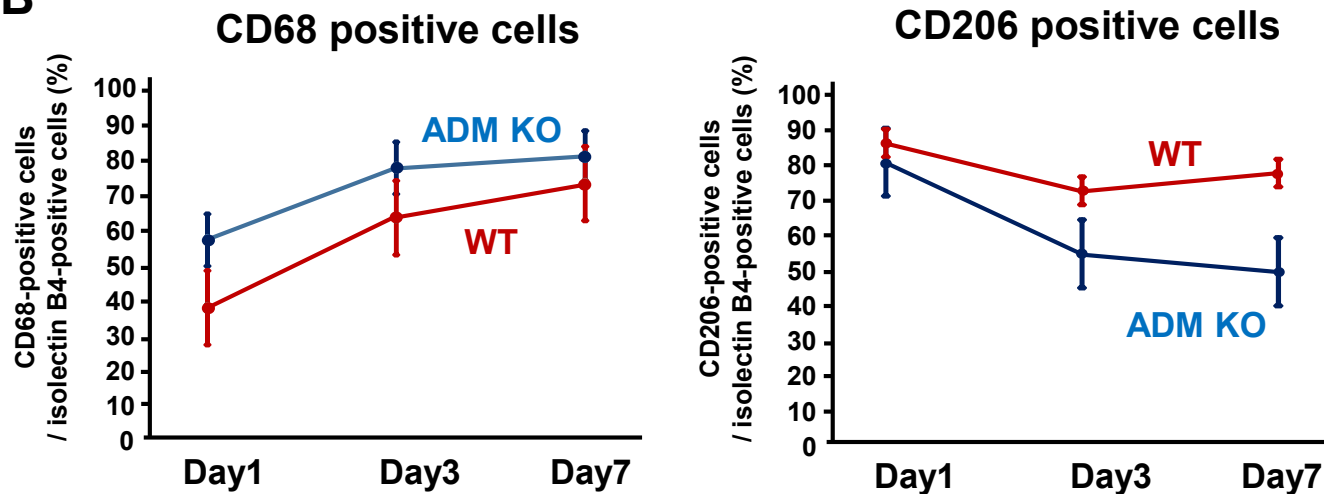


Figure 8

A**B****Figure 9**

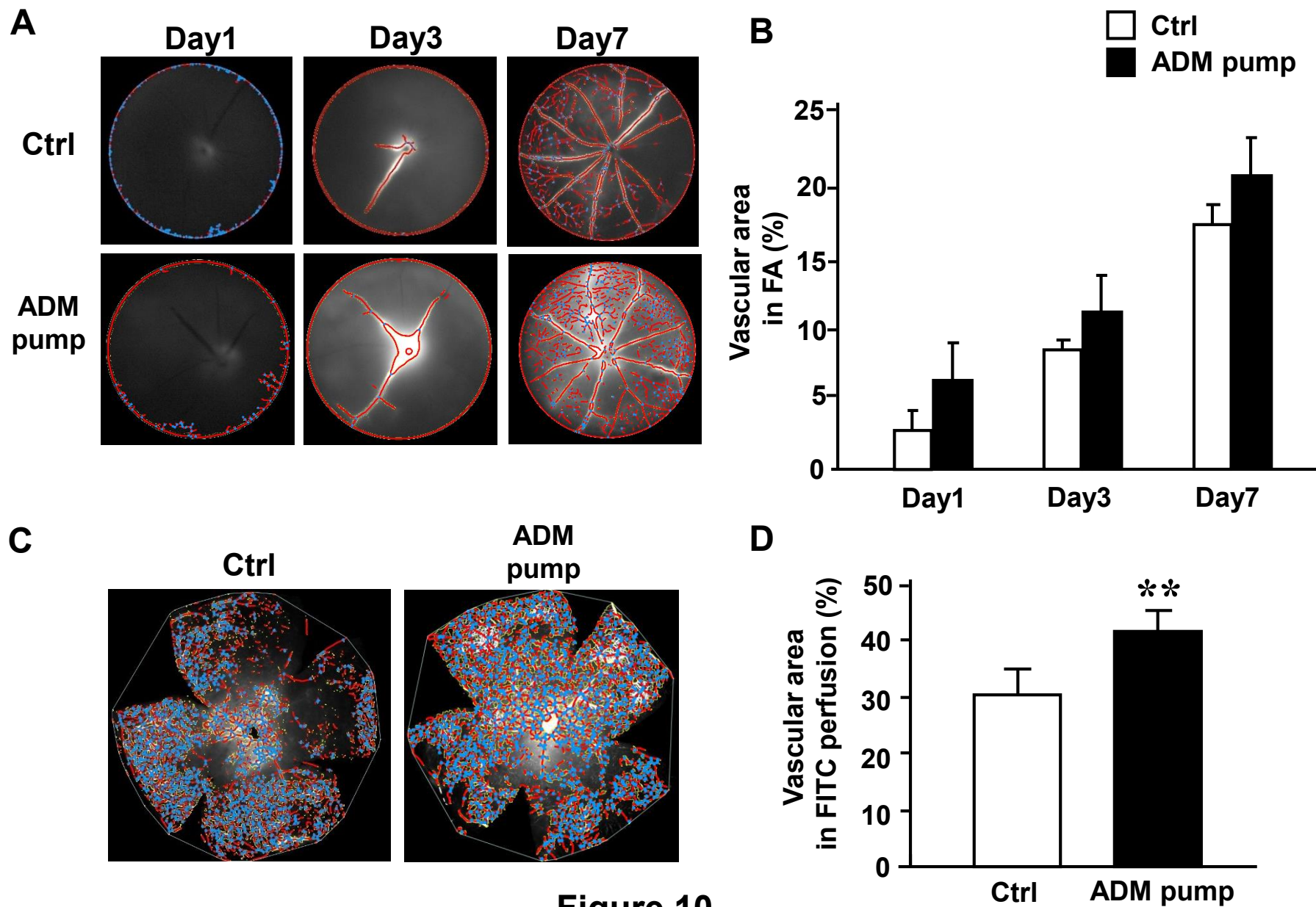
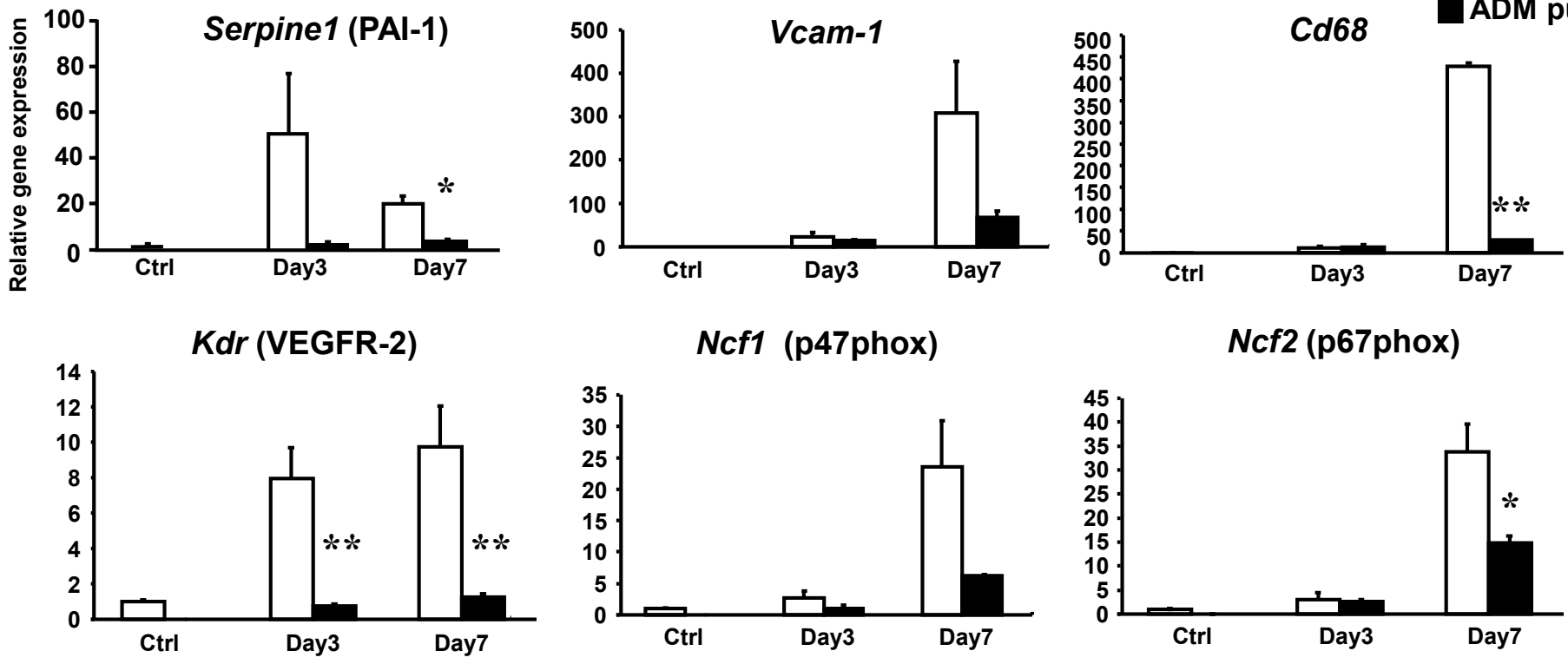
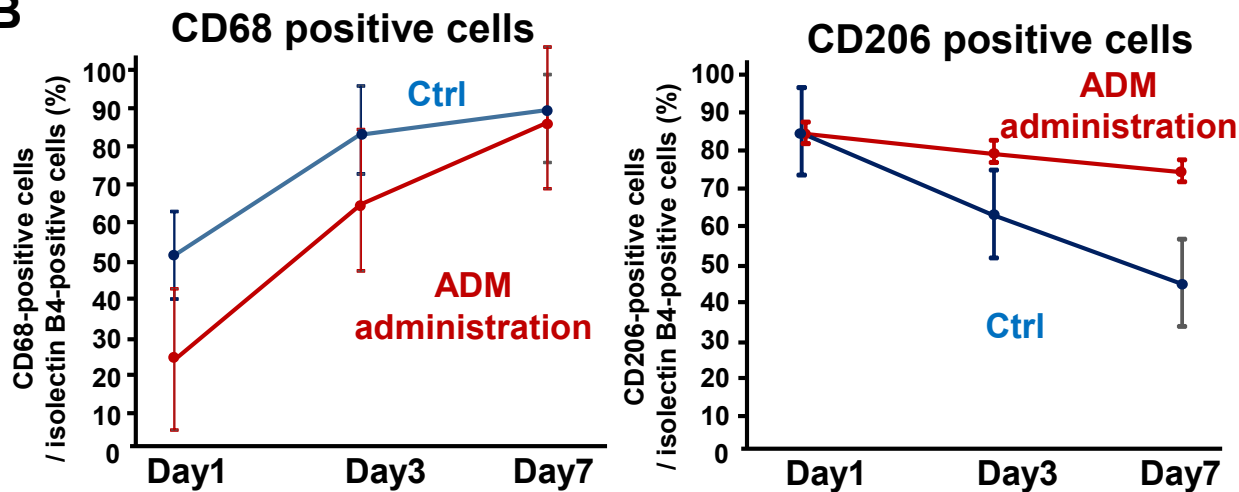


Figure 10

A

□ Ctrl
 ■ ADM pump

**B****Figure 11**

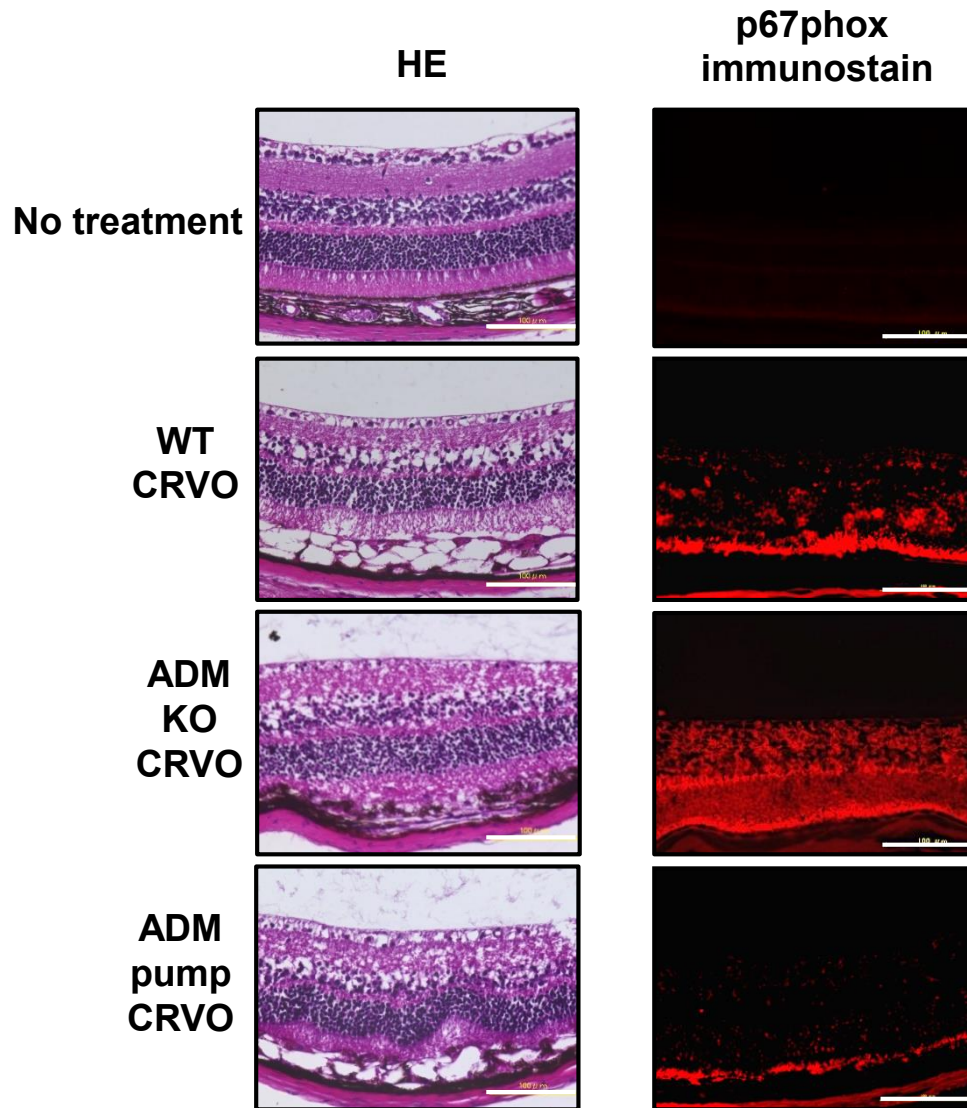


Figure 12

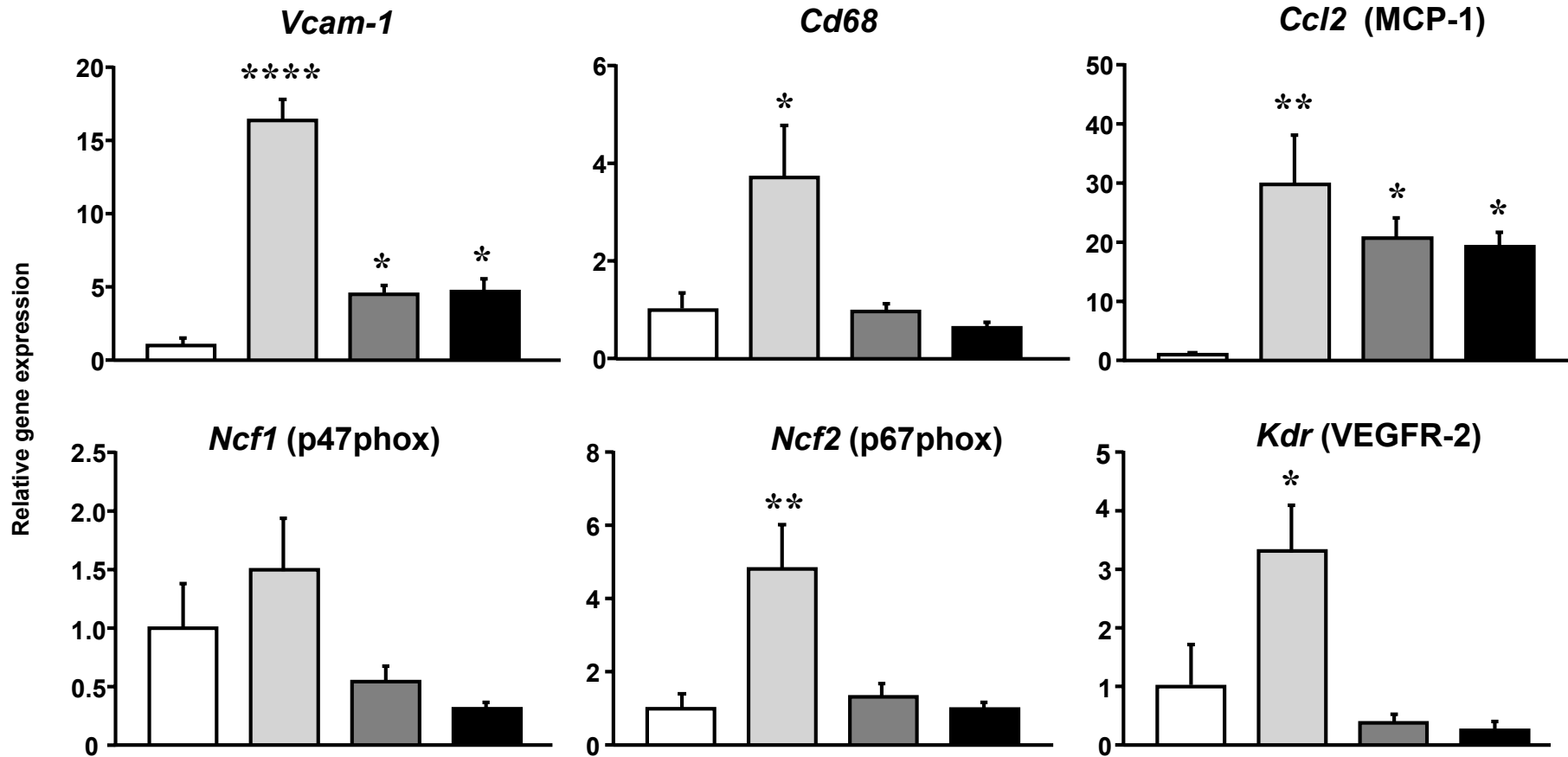
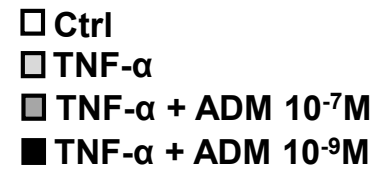


Figure 13

Virchow's triad

ADM-RAMP2 system

Vasodilatation

Anti-coagulation

Anti-hyperpermeability
Anti-inflammation
Anti-oxidative stress

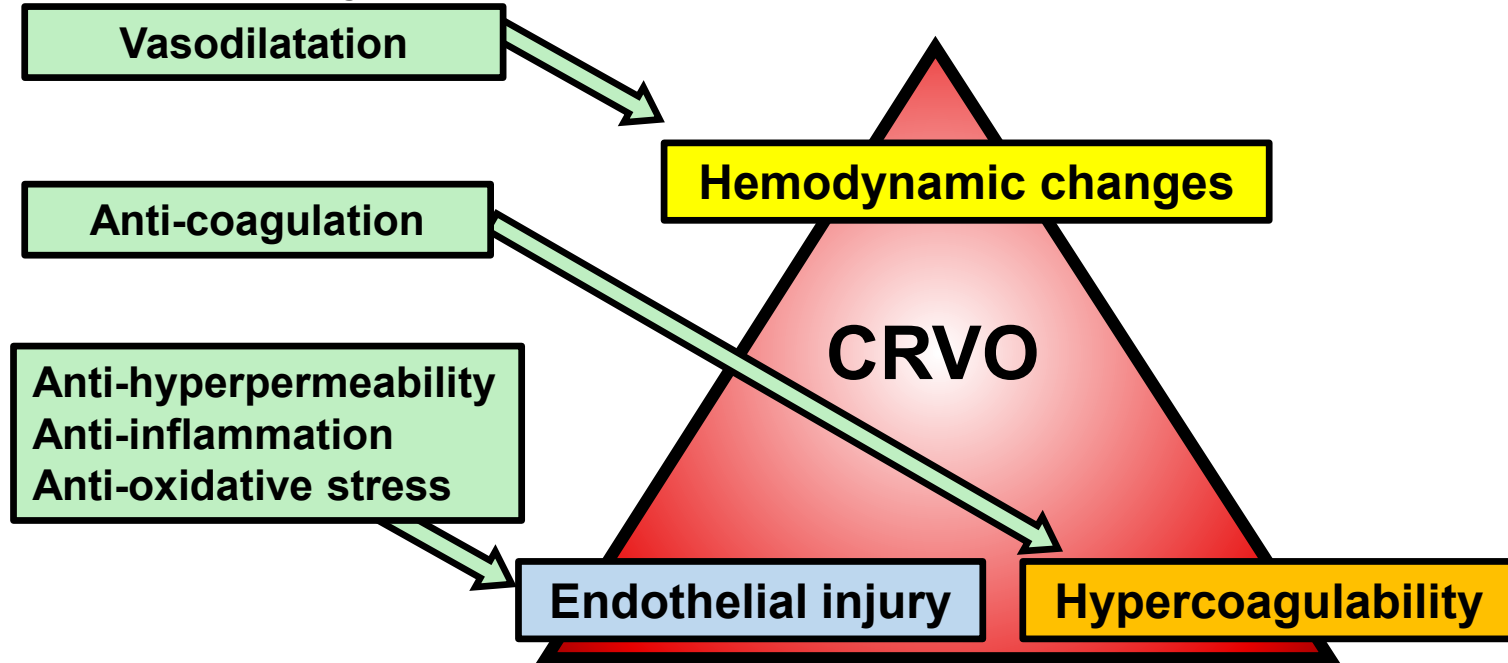
Hemodynamic changes

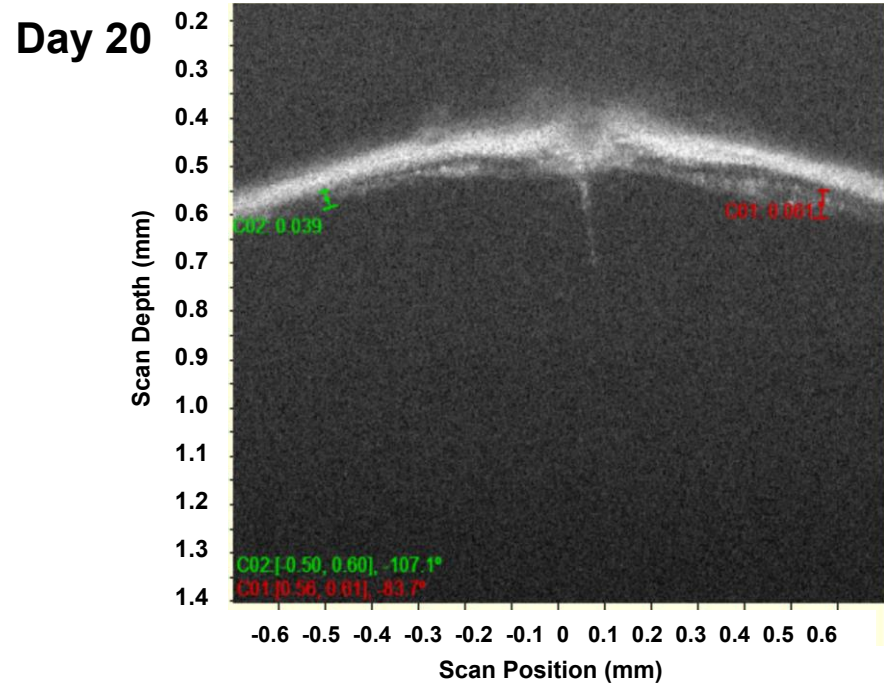
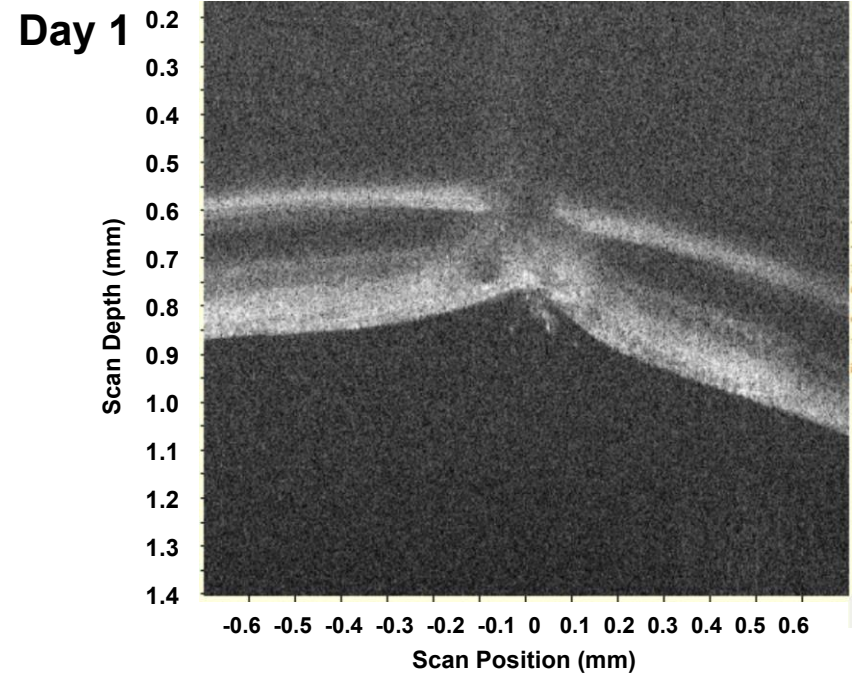
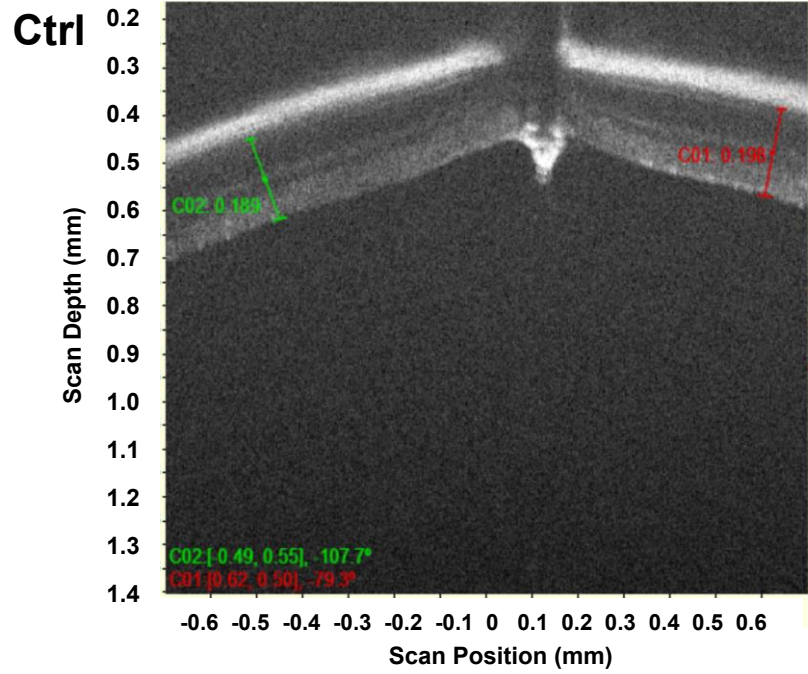
CRVO

Endothelial injury

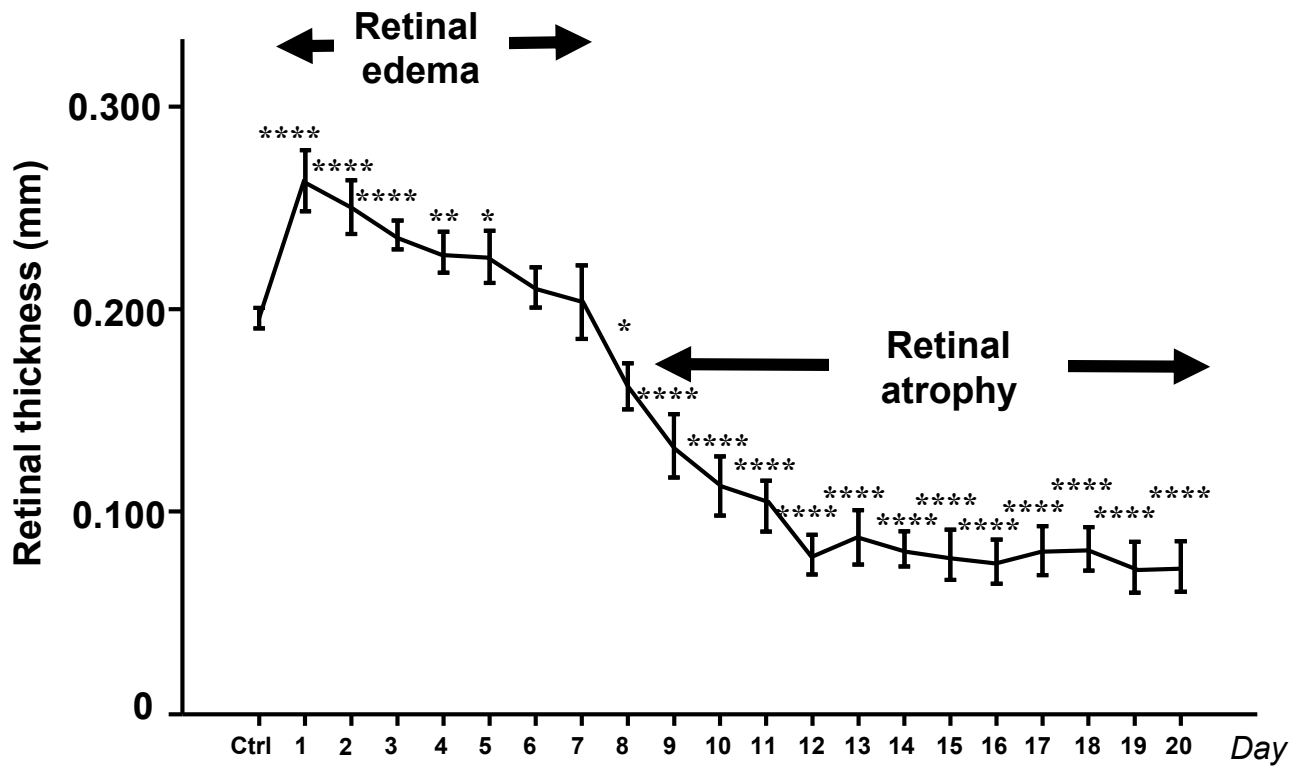
Hypercoagulability

Figure 14

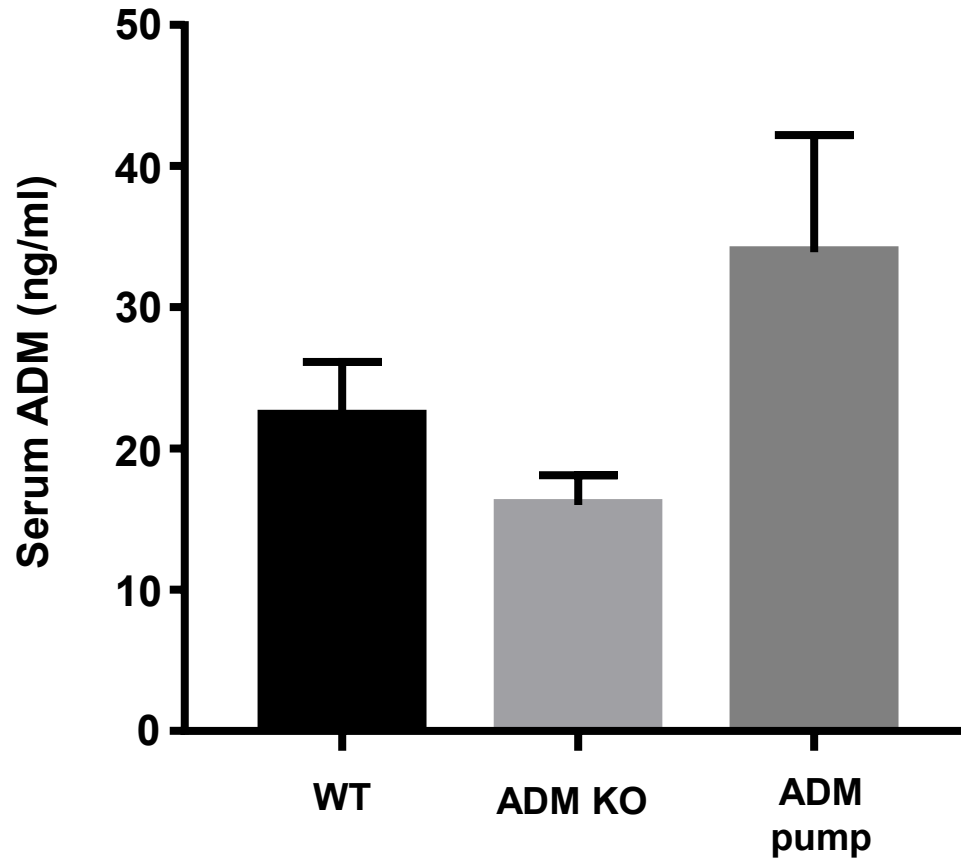




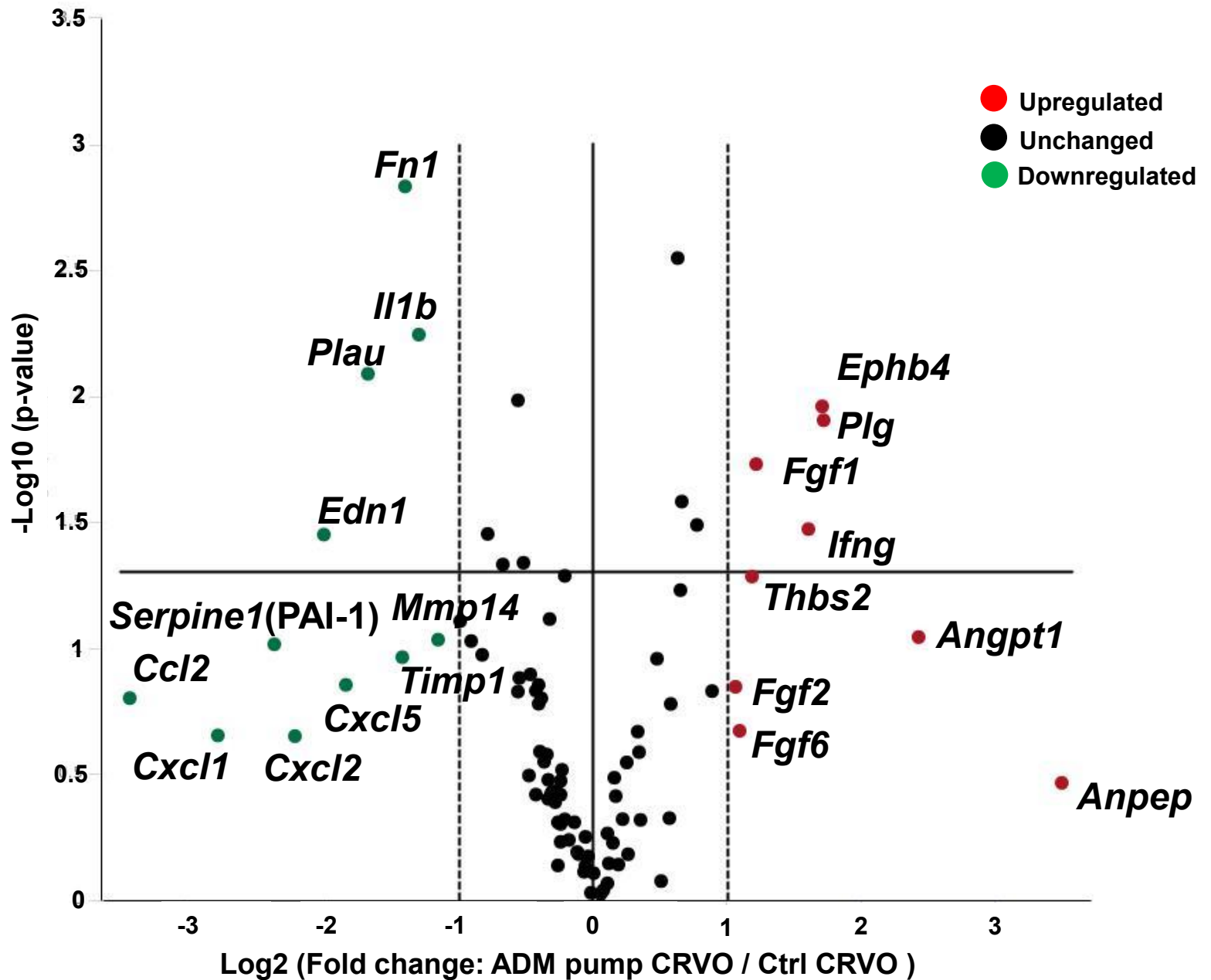
Supplementary Figure 1



Supplementary Figure 2



Supplementary Figure 3



Supplementary Figure 4